

Point-group selection rules and universal momentum-transfer dependencies for inelastic neutron scattering on molecular spin clusters

Shadan Ghassemi Tabrizi **Technische Universität Berlin, Institut für Chemie, Theoretische Chemie, Sekr. C7, Strasse des 17. Juni 135, 10623 Berlin, Germany*

(Received 13 February 2021; revised 16 April 2021; accepted 26 May 2021; published 10 June 2021)

Recent significant progress in inelastic neutron scattering (INS) has rendered this technique even more useful for the characterization of magnetic systems, including molecular spin clusters. By so-called four-dimensional INS on single-crystal probes, excitation spectra can be recorded in large portions of momentum-transfer (\mathbf{Q}) and energy-transfer (E) space. Spin-selection rules permit $\Delta S = 0, \pm 1$ transitions between different spin multiplets. Additional selection rules can be imposed by point-group symmetry but were not discussed yet. As most synthetic spin clusters with interesting magnetic properties have high molecular symmetry, a clear understanding of this issue will be helpful for interpreting INS spectra. Here we discuss point-group INS selection rules for magnetically isotropic or anisotropic spin clusters. Rings and a number of spin polyhedra with cubic or icosahedral symmetry are chosen as illustrative and relevant examples. These systems exhibit a significant number of point-group selection rules in isotropic spin models, and most of them maintain a smaller number of selection rules in anisotropic spin models. We also explain how the \mathbf{Q} dependence of certain excitations depends exclusively on the point-group symmetry of the states involved in the transition, an aspect that had thus far only been detailed for spin rings. We provide the universal \mathbf{Q} -dependent intensity functions (and their powder-averaged forms) for a set of polyhedra (cube, icosahedron, truncated tetrahedron, cuboctahedron, dodecahedron, icosidodecahedron, and truncated icosahedron). Overall, these results help to disentangle the relevant dynamical information contained in INS spectra from those features that are entirely determined by molecular symmetry.

DOI: [10.1103/PhysRevB.103.214422](https://doi.org/10.1103/PhysRevB.103.214422)

I. INTRODUCTION

The rich set of magnetic properties and phenomena observed in exchange-coupled spin clusters [1–3] has opened up the prospect of using magnetic molecules in future technology, including quantum computing [4–9], high-density data storage [10–12], magnetic cooling [13], or spintronics devices [14]. Inelastic neutron scattering (INS) is a key experimental technique for studying magnetic excitations in such systems. At an early stage, INS was applied to study exchange interactions in dimers and other small spin clusters [15–17]. More recently, INS played an important role in determining the microscopic interactions (effectively represented by spin-Hamiltonian parameters) of molecular spin clusters, including nanomagnets, antiferromagnetic spin rings, and other systems (see Refs. [18–22] for reviews). With a single exception [23], powder probes were used. In this way, only the dependence of the INS intensity on energy transfer (E) and the magnitude of momentum transfer (Q) could be investigated. Recent dramatic progress in instrumentation (the installation of new spectrometers or detectors), new tools for data analysis, and the availability of sufficiently large single crystals now permits four-dimensional (4D) INS experiments, where the three-dimensional (3D) momentum-transfer vector \mathbf{Q} can be measured [22]. That is, the INS cross section becomes a

function of E and \mathbf{Q} instead of just E and Q , and this facilitates the extraction of information on spin dynamics. 4D-INS has already provided detailed insights into the physics of various spin clusters [22,24–28], and the possibilities of this technique are expected to further expand in the future [21,22]. It is worth noting that quantum computers were demonstrated to be useful for simulating 4D-INS spectra [29], which could become an interesting option for systems that are too large for exact diagonalization of the spin Hamiltonian. However, the present work is focused on those features of the INS cross section which are fixed by molecular symmetry, where exact or approximate eigenstates are not needed.

Isotropic exchange is usually the dominant contribution to the spin Hamiltonian of first-row transition-metal spin clusters [1]. Owing to the $\Delta S = 0, \pm 1$ spin-selection rule, INS transitions between different spin multiplets yield information on exchange-coupling constants. It is well known that additional selection rules arise if the magnitude of the total spin of a subset of sites is conserved (see comments and references in the Theory section). However, more general selection rules deriving from the point-group symmetry were not considered. We are aware of only one work which very briefly touches on this issue [30].

Here, we discuss INS selection rules imposed by molecular symmetry in isotropic and anisotropic systems. The isotropic systems are symmetric under permutations of sites [31]. Anisotropic Hamiltonians generally break permutation and spin symmetry, but combinations of permutations and

*ghastab@mailbox.tu-berlin.de

spin rotations according to operations of the molecular point group still represent symmetries and may impose constraints on INS transition-matrix elements. Spin rings and a number of polyhedra (cube, icosahedron, truncated tetrahedron, cuboctahedron, dodecahedron, icosidodecahedron, and truncated icosahedron) are chosen as illustrative examples.

The \mathbf{Q} dependence is sometimes completely determined by the symmetry species of the states involved in the INS transition [32]. Then exact eigenstates are required only to calculate the absolute intensity. The detailed analysis in Ref. [32] was limited to cyclic systems. Our generalized analysis (see Theory section) leads to Eq. (13), which is a main result of the present work. For the indicated isotropic spin polyhedra, we tabulate and plot all universal \mathbf{Q} -dependent functions in Results and Discussion. This information should be useful for interpreting high-resolution INS spectra of the given types of systems (and the outlined simple formalism can be used to derive the respective information for other species, too), which will conceivably become available by future combined synthetic and experimental efforts.

II. THEORY

Spin Hamiltonian. The determination of the J_{ij} coupling constants that parameterize the isotropic Heisenberg Hamiltonian,

$$\hat{H}^{(0)} = \sum_{i<j} J_{ij} \hat{\mathbf{S}}_i \cdot \hat{\mathbf{S}}_j, \quad (1)$$

is a major goal of many INS studies. Besides $SU(2)$ spin-rotational symmetry, an isotropic spin Hamiltonian (which may include also biquadratic exchange, three-center terms, etc.) is symmetric under site permutations that correspond to real-space symmetry transformations of the cluster. Spin-permutational symmetry (SPS, [31]) is a manifestation of molecular symmetry and leads to a point-group classification of exchange multiplets [33]. Note, however, that the SPS group sometimes represents only a subgroup of the full point group of a molecule, as discussed by Waldmann [31]. For example, for a planar spin ring with N sites and a D_{Nh} molecular point group, $\hat{H}^{(0)}$ has SPS symmetry D_N , while the full D_{Nh} group becomes relevant for a general anisotropic spin model (see below). The simple SPS symmetry remains intact when uniaxial anisotropy terms (conserving \hat{S}_z) are included [31]. In numerical studies, combining SPS with \hat{S}_z is highly useful for block-diagonalizing the Hamiltonian [31,34,35]. Even smaller blocks are obtained when adapting the basis to the full $SU(2)$ spin symmetry ($\hat{\mathbf{S}}^2$ and \hat{S}_z) [1,36], but a combination of $SU(2)$ with SPS is technically considerably more demanding [31,37,38]. In a sense, the symmetry labels of energy eigenstates are obtained as a byproduct and provide valuable qualitative information on spectroscopic transitions (as well as selection rules for anisotropy-induced spin mixing [30,39], and other properties [40,41]), where the INS technique is of central interest to the present work.

The reliable determination of anisotropic interactions by experiments or quantum-chemical calculations remains challenging. For ions with $s_i > \frac{1}{2}$, single-ion zero-field splitting (ZFS) is often most important (taking the form $\hat{\mathbf{S}}_i \cdot \mathbf{D}_i \cdot \hat{\mathbf{S}}_i$, with a traceless symmetric ZFS tensor \mathbf{D}_i). Further common terms

are symmetric ($\hat{\mathbf{S}}_i \cdot \mathbf{D}_{ij} \cdot \hat{\mathbf{S}}_j$) and antisymmetric ($\mathbf{d}_{ij} \cdot \hat{\mathbf{S}}_i \times \hat{\mathbf{S}}_j$) coupling between nearest neighbors (NN). The orientation of a vector \mathbf{d}_{ij} is fixed with respect to specific symmetry elements [1,42], and in high-symmetry systems (including many polyhedra), antisymmetric exchange is overall excluded ($\mathbf{d}_{ij} = 0$). On the other hand, symmetric couplings are never excluded on account of point-group symmetry (although they were apparently claimed to be absent in spin tetrahedra [43]). One may consider $\hat{H}^{(1)}$ as defined in Eq. (2),

$$\hat{H}^{(1)} = \sum_{i<j} \hat{\mathbf{S}}_i \cdot \mathbf{D}_{ij} \cdot \hat{\mathbf{S}}_j, \quad (2)$$

where (up to a factor that can be different for different types of spin pairs) \mathbf{D}_{ij} is a traceless symmetric tensor of rank 2,

$$\mathbf{D}_{ij} = \mathbf{n}_{ij} \mathbf{n}_{ij}^T - \frac{1}{3} \mathbf{1}, \quad (3)$$

with the unit vector $\mathbf{n}_{ij} = \mathbf{R}_{ij}/|\mathbf{R}_{ij}|$ pointing from site i to site j . This affords an anisotropic spin Hamiltonian which is in accord with the point-group symmetry of the cluster. However, the specific form of anisotropic contributions is not relevant here.

$SU(2)$ and SPS symmetry are each broken by general anisotropic interactions as represented, e.g., by Eqs. (2) and (3). However, when the SPS operations are combined with appropriate spin rotations, one recovers the symmetry group of the anisotropic Hamiltonian [39,43,44]. Point-group labels can still be attached to eigenstates, and INS selection rules may ensue, as explained below. We only mention in passing that a Zeeman term would completely break the symmetries of anisotropic spin Hamiltonians, unless the magnetic field is applied along a symmetry axis or perpendicular to a symmetry plane (inversion symmetry stays intact for arbitrary field orientations) [39].

INS point-group selection rules. The differential neutron-scattering cross section is given by Eq. (4) [32,45],

$$\frac{d^2\sigma}{d\Omega d\omega} = \frac{\gamma e^2 k'}{m_e c^2 k} e^{-2W(\mathbf{Q},T)} \times \sum_{n,m} \frac{e^{-E_n/kT}}{q(T)} I_{nm}(\mathbf{Q}) \delta\left(\omega - \frac{E_m - E_n}{\hbar}\right), \quad (4)$$

where Ω denotes the solid angle, $\hbar\omega$ is the energy transfer, $\mathbf{Q} = \mathbf{k} - \mathbf{k}'$ is the scattering vector, $e^{-2W(\mathbf{Q},T)}$ is the Debye-Waller factor, $e^{-E_n/kT}/q(T)$ is the Boltzmann factor, and all other symbols have their usual meaning. $I_{nm}(\mathbf{Q})$ is defined in Eq. (5),

$$I_{nm}(\mathbf{Q}) = \sum_{i,j} F_i^*(Q) F_j(Q) e^{i\mathbf{Q} \cdot (\mathbf{R}_i - \mathbf{R}_j)} \times \sum_{\alpha,\beta} \left(\delta_{\alpha\beta} - \frac{Q_\alpha Q_\beta}{Q^2} \right) \langle n | \hat{s}_{i\alpha} | m \rangle \langle m | \hat{s}_{j\beta} | n \rangle, \quad (5)$$

where $\alpha, \beta = x, y, z$, and \mathbf{R}_i is the position vector of the i th spin center (the sums over i and j independently run over all N sites), and $|n\rangle$ and $|m\rangle$ are energy eigenstates. For transition-metal ions with a rather localized and isotropic spin density, it is a good approximation to treat the magnetic form factor as isotropic, $F_i(\mathbf{Q}) = F_i(Q)$ (but other open-shell species can have significant anisotropy [46]). Overall, for INS

experiments conducted on molecular spin clusters thus far, the dependence of the cross section on the orientation of \mathbf{Q} can be taken to be contained in $I_{nm}(\mathbf{Q})$, Eq. (5) [21]. A spherical average must be taken for powder samples [16,32],

$$\bar{I}_{nm}(\mathbf{Q}) \equiv \int \frac{I_{nm}(\mathbf{Q})}{4\pi} d\Omega. \quad (6)$$

For isotropic systems, this yields Eq. (7) [32],

$$\bar{I}_{nm}(\mathbf{Q}) = \frac{2}{3} \sum_{i,j} F_i^*(\mathbf{Q}) F_j(\mathbf{Q}) j_0(QR_{ij}) \sum_{\alpha} \langle n|\hat{s}_{i\alpha}|m\rangle \langle m|\hat{s}_{j\alpha}|n\rangle, \quad (7)$$

where $j_0(x) = \sin(x)/x$ is a spherical Bessel function, and $R_{ij} = |\mathbf{R}_i - \mathbf{R}_j|$ (Ref. [32] also derives $\bar{I}_{nm}(\mathbf{Q})$ for anisotropic systems). For simplicity, ignoring the other factors in Eq. (4), we call $I_{nm}(\mathbf{Q})$ and $\bar{I}_{nm}(\mathbf{Q})$ the single-crystal and powder INS intensity, respectively. The spin-selection rules ($\Delta S = 0, \pm 1$, $\Delta M = 0, \pm 1$; transitions $S = 0 \rightarrow S = 0$ are not allowed) are set by the conditions under which a matrix element $\langle n|\hat{s}_{i\alpha}|m\rangle$ vanishes. However, $\langle n|\hat{s}_{i\alpha}|m\rangle$ can also vanish on account of point-group symmetry.

Suppose that states $|n\rangle$ and $|m\rangle$ transform according to irreducible representations Γ_n and Γ_m of the SPS group, respectively. The N -site spin operators $\{\hat{s}_i\}$ span the (generally reducible) N -dimensional representation $\Gamma^{(N)}$. (Cartesian components α of operators $\hat{s}_{i\alpha}$ are not affected by permutations, but they are mixed when permutations are combined with spin rotations, see the discussion on selection rules in anisotropic systems below.) Then all $\langle n|\hat{s}_{i\alpha}|m\rangle$ vanish, if $\Gamma_n^* \times \Gamma^{(N)} \times \Gamma_m$ does not contain the totally symmetric representation Γ_1 . The determination of selection rules is thus straightforward, requiring only the direct-product table for the SPS group in addition to the decomposition of $\Gamma^{(N)}$ in terms of irreducible representations.

For certain coupling topologies, the isotropic spin Hamiltonian is left invariant by all permutations within a subset of sites, such that the squared total spin of the subsystem becomes a good quantum number. This applies, for example, to individual pairs in equilateral triangles, the square, and other systems; INS transitions are limited to changes of the total spin of a subsystem by 0 or 1 units [47–50], where in the presence of several subsystems (e.g., two dimers in a square), the total spin of only one subsystem may change in the transition. Although a well-defined subsystem spin can be a manifestation of molecular symmetry, we do not count the resulting selection rules as genuine point-group selection rules in the general sense but rather classify them as combined spin- and point-group selection rules.

Anisotropic systems are somewhat more complicated. As explained in detail elsewhere [39,43,44], spin permutations must be combined with global spin rotations to leave the anisotropic zero-field Hamiltonian invariant. For systems with even spin (meaning that $2 \sum_i s_i$ is an even number), eigenstates can be labeled with respect to the molecular point group, but the respective double group must be considered for odd-spin systems (where $2 \sum_i s_i$ is an odd number) [44]. The determination of selection rules again requires analysis of the representation spanned by $\{\hat{s}_i\}$. However, spin rotations mix Cartesian components so that symmetry operations are

represented by matrices of dimension $3N \times 3N$ (instead of $N \times N$ in the isotropic case). The decomposition of the $\{\hat{s}_i\}$ basis thus becomes similar to a symmetry classification of vibrational, rotational, and translational modes in molecules [51]. If $\Gamma_n^* \times \Gamma^{(3N)} \times \Gamma_m$ does not contain Γ_1 , all $\langle n|\hat{s}_{i\alpha}|m\rangle$ vanish. Additional details are discussed for specific examples in Results and Discussion.

Q dependence determined by SPS symmetry. Waldmann has shown that in certain isotropic systems the \mathbf{Q} dependence of the INS intensity $I_{nm}(\mathbf{Q})$ is completely fixed by the symmetry species Γ_n and Γ_m [32]. Symmetric spin rings were considered in detail [32]. In the cyclic or dihedral groups (C_N or D_N), $I_{nm}(\mathbf{Q})$ takes a universal form (up to a multiplicative constant) for given Γ_n and Γ_m , irrespective of the uniform local quantum number s . More complicated groups were not discussed. Our consideration of point-group selection rules offers the opportunity to investigate this issue in more detail, as explained in the following.

To simplify the discussion, we consider unpolarized transitions by summing up intensities for transitions between all pairs of magnetic states belonging to the two different spin multiplets. We also sum over components k_n and k_m of Γ_n and Γ_m , respectively (for multidimensional SPS representations). The resulting total sum is denoted by $I_{\Gamma_n \Gamma_m}(\mathbf{Q})$. Assuming that all sites are equivalent, we define $I_{\Gamma_n \Gamma_m}(\mathbf{Q}) = |F(\mathbf{Q})|^2 L_{\Gamma_n \Gamma_m}(\mathbf{Q})$. Apart from a factor (which is irrelevant for our discussion), the Wigner-Eckart theorem allows us to write $L_{\Gamma_n \Gamma_m}(\mathbf{Q})$ in terms of reduced matrix elements (RMEs) of the $\hat{\mathbf{T}}^{(1)}(\mathbf{s}_i)$ rank-1 irreducible tensor operators (ITOs),

$$L_{\Gamma_n \Gamma_m}(\mathbf{Q}) = \sum_{i,j} e^{i\mathbf{Q} \cdot (\mathbf{R}_i - \mathbf{R}_j)} \sum_{k_n, k_m} \langle \Gamma_n, k_n \| \hat{\mathbf{T}}^{(1)}(\mathbf{s}_i) \| \Gamma_m, k_m \rangle \times \langle \Gamma_m, k_m \| \hat{\mathbf{T}}^{(1)}(\mathbf{s}_j) \| \Gamma_n, k_n \rangle. \quad (8)$$

The polarization factor, $\delta_{\alpha\beta} - Q_\alpha Q_\beta / Q^2$, cf. Eq. (5), has been averaged out by the combined summation over magnetic quantum numbers of both multiplets. We stress that n and m denote different spin multiplets, but they may both have the same SPS symmetry (that is, our discussion is valid for both $\Gamma_n \neq \Gamma_m$ and $\Gamma_n = \Gamma_m$).

The $\{\hat{s}_i\}$ basis spans Γ_1 exactly once. In obvious notation,

$$\hat{\mathbf{T}}_{\Gamma_1} = \frac{1}{\sqrt{N}} \sum_i \hat{\mathbf{T}}(\mathbf{s}_i) = \frac{1}{\sqrt{N}} \hat{\mathbf{T}}(\mathbf{S}), \quad (9)$$

where $\hat{\mathbf{T}}(\mathbf{S})$ refers to the total spin, $\hat{\mathbf{S}} = \sum_i \hat{s}_i$ (here and in the following, the rank-1 superscript on ITOs was dropped to avoid clutter). Matrix elements between states belonging to different spin multiplets vanish, $\langle \Gamma_n, k_n \| \hat{\mathbf{T}}(\mathbf{S}) \| \Gamma_m, k_m \rangle = 0$, due to spin symmetry. In other words, INS transitions cannot be caused by the $\hat{\mathbf{T}}_{\Gamma_1}$ transition operator. This is a combined spin- and point-group selection rule.

Let Γ denote the representation spanned by $\{\hat{s}_i\}$, where we exclude Γ_1 from Γ . We shall assume that Γ contains exactly one irreducible representation Γ_l such that $\Gamma_n^* \times \Gamma_l \times \Gamma_m$ contains Γ_1 , and we further assume that Γ_l occurs exactly one time in Γ . A unitary matrix \mathbf{v} mediates the transformation from the local basis $\{\hat{s}_i\}$ to the symmetry-adapted

basis,

$$\hat{\mathbf{T}}_{\Gamma_q k_q} = \sum_i v_{\Gamma_q k_q, i} \hat{\mathbf{T}}(\mathbf{s}_i), \quad (10)$$

where $\Gamma_q k_q$ is a compound index ($\Gamma_q k_q = 1, 2, \dots, N$) which can include a specific irreducible representation more than once. The reverse transformation is given in Eq. (11),

$$\hat{\mathbf{T}}(\mathbf{s}_i) = \sum_{\Gamma_q k_q} v_{\Gamma_q k_q, i}^* \hat{\mathbf{T}}_{\Gamma_q k_q}. \quad (11)$$

Inserting Eq. (11) into Eq. (8) and using the assumption that only $\hat{\mathbf{T}}_{\Gamma_l k_l}$ transition operators can have nonvanishing matrix elements gives us Eq. (12):

$$L_{\Gamma_n \Gamma_m}(\mathbf{Q}) = \sum_{i, j} e^{i\mathbf{Q} \cdot (\mathbf{R}_i - \mathbf{R}_j)} \sum_{k_l, k'_l, k_m, k_n} v_{\Gamma_l k_l, i}^* v_{\Gamma_l k'_l, j}^* \langle \Gamma_n, k_n \| \hat{\mathbf{T}}_{\Gamma_l k_l} \| \Gamma_m, k_m \rangle \langle \Gamma_m, k_m \| \hat{\mathbf{T}}_{\Gamma_l k'_l} \| \Gamma_n, k_n \rangle. \quad (12)$$

We ultimately employ the Wigner-Eckart theorem for point groups [52,53] to factor out the dependence of spin RMEs on the combination of components (k_l, k'_l, k_m, k_n) of multidimensional SPS representations,

$$L_{\Gamma_n \Gamma_m}(\mathbf{Q}) = \langle \Gamma_n \| \hat{\mathbf{T}}_{\Gamma_l} \| \Gamma_m \rangle \langle \Gamma_m \| \hat{\mathbf{T}}_{\Gamma_l} \| \Gamma_n \rangle \times \sum_{i, j} e^{i\mathbf{Q} \cdot (\mathbf{R}_i - \mathbf{R}_j)} \sum_{k_l} v_{\Gamma_l k_l, i}^* v_{\Gamma_l k_l, j}, \quad (13)$$

where the double-bar matrix elements $\langle \Gamma_n \| \hat{\mathbf{T}}_{\Gamma_l} \| \Gamma_m \rangle$ now denote combined spin- and SPS-RMEs (which are again left undefined up to an irrelevant factor). Note the single complex-conjugation sign in $v_{\Gamma_l k_l, i}^* v_{\Gamma_l k_l, j}$. Equation (13) refers to the case where $\Gamma_n^* \times \Gamma_m$ contains Γ_l exactly once. In nonsimple groups, Γ_l can occur multiple times in $\Gamma_n^* \times \Gamma_m$ (e.g., in the I_h group, $F_g \times H_g$ contains H_g twice, etc.) [53]. Then the prefactor in Eq. (13) would be a linear combination of RME products (cf. Ref. [54] on the generalized Wigner-Eckart theorem). However, the important \mathbf{Q} -dependent part of Eq. (13) is not affected in such cases.

Equation (13) generalizes the results of Waldmann [32] and is a central result of the present work. Equation (13) shows that only the total intensity requires dynamical information in terms of the RMEs, whereas the \mathbf{Q} dependence is completely determined by the SPS symmetry labels Γ_n and Γ_m (which determine Γ_l), irrespective of the local spin quantum number s . We define $K_{\Gamma_l}(\mathbf{Q})$ to be the \mathbf{Q} -dependent factor for transitions mediated by the Γ_l transition operator,

$$K_{\Gamma_l}(\mathbf{Q}) = \sum_{i, j} e^{i\mathbf{Q} \cdot (\mathbf{R}_i - \mathbf{R}_j)} \sum_{k_l} v_{\Gamma_l k_l, i}^* v_{\Gamma_l k_l, j}. \quad (14)$$

Defining $w_{\Gamma_l k_l, i} = e^{-i\mathbf{Q} \cdot \mathbf{R}_i} v_{\Gamma_l k_l, i}$, we can write $K_{\Gamma_l}(\mathbf{Q})$ more compactly,

$$K_{\Gamma_l}(\mathbf{Q}) = \sum_{i, j} \sum_{k_l} w_{\Gamma_l k_l, i}^* w_{\Gamma_l k_l, j}. \quad (15)$$

In summary, Eq. (13) was obtained for an isotropic spin system where all sites are equivalent, where Γ contains exactly one Γ_l (with Γ_l occurring just once), such that $\Gamma_n^* \times \Gamma_m$ contains Γ_l , and n and m denote different spin

multiplets. (A magnetically unpolarized transition was only assumed for notational convenience, see comments above; polarized transitions would still need to take into account the polarization factor.) If these conditions are not met, the \mathbf{Q} dependence of the INS intensity is generally not fixed by symmetry and will require a certain amount of dynamical information. (However, in a few cases, systems that host sets of spin sites which are not equivalent by symmetry may still have transitions characterized by a definite $K_{\Gamma_l}(\mathbf{Q})$ or $\tilde{K}_{\Gamma_l}(Q)$; see the discussion on symmetry breaking in the Results section for spin rings, the cube, and the icosahedron.) Regarding the dynamical information required to define \mathbf{Q} dependencies for transitions that are not characterized by a universal $K_{\Gamma_l}(\mathbf{Q})$, for simplicity we shall consider the special case where Γ_l occurs h times in Γ ($h > 1$), assuming further that Γ_l , Γ_m , and Γ_n are one-dimensional. The rank-1 ITOs $\hat{\mathbf{T}}_{\Gamma_l}^p$, $p = 1, 2, \dots, h$, are defined by a set of orthogonal vectors $\mathbf{v}_{\Gamma_l}^p$. Thus from Eq. (12),

$$L_{\Gamma_n \Gamma_m}(\mathbf{Q}) = \sum_{i, j} e^{i\mathbf{Q} \cdot (\mathbf{R}_i - \mathbf{R}_j)} \sum_{p, p'} (v_{\Gamma_l, i}^p)^* v_{\Gamma_l, j}^{p'} \times \langle \Gamma_n \| \hat{\mathbf{T}}_{\Gamma_l}^p \| \Gamma_m \rangle \langle \Gamma_m \| \hat{\mathbf{T}}_{\Gamma_l}^{p'} \| \Gamma_n \rangle, \quad (16)$$

which does not factorize into a \mathbf{Q} -dependent and an RME part. Thus the least amount of dynamical information required to describe the \mathbf{Q} dependence, for $h = 2$, is a ratio of two RMEs, $\langle \Gamma_m \| \hat{\mathbf{T}}_{\Gamma_l}^1 \| \Gamma_n \rangle / \langle \Gamma_m \| \hat{\mathbf{T}}_{\Gamma_l}^2 \| \Gamma_n \rangle$.

In the Results and Discussion section, we tabulate those transition types (characterized by Γ_n and Γ_m) which are associated with a unique $K_{\Gamma_l}(\mathbf{Q})$ and list analytical expressions for the $K_{\Gamma_l}(\mathbf{Q})$ functions for a number of spin polyhedra with cubic or icosahedral symmetry. We lastly mention that in ferromagnetic spin clusters with uniaxial anisotropy of Ising type, the zero-temperature excitations observable in INS can be found in the $M = \pm(S_{\max} - 1)$ sector (where M is the \hat{S}_z eigenvalue and $S_{\max} = \sum_i s_i$; the ground state has $M = \pm S_{\max}$) [55]. Due to its connection to concepts familiar from extended magnetic systems, a simple formalism for gaining an intuitive and pictorial understanding of such excitations has been termed ferromagnetic cluster spin-wave theory (FCSWT) [55]; see Refs. [56,57] for applications to INS. The ferromagnetic ($M = S_{\max}$) ground state transforms as Γ_1 , while the $(N-1)$ different excited states ($M = S_{\max} - 1$) span Γ (that is, the representation spanned by $\{\hat{s}_i\}$, excluding Γ_1). This implies that all possible $K_{\Gamma_l}(\mathbf{Q})$ functions can be found among the (zero-temperature) FCSWT transitions. Therefore our Eq. (14) for $K_{\Gamma_l}(\mathbf{Q})$ is formally equivalent to equations describing the \mathbf{Q} dependence in FCSWT transitions (cf. Ref. [56]), although we have here derived it in a broader context. For the spin polyhedra studied in Results and Discussion, this analogy with FCSWT has prompted us to additionally report analytical expressions for \mathbf{Q} dependencies for all FCSWT transitions, including those that are not associated with a universal $K_{\Gamma_l}(\mathbf{Q})$ function (this applies to those Γ_l that occur more than once in Γ).

III. RESULTS AND DISCUSSION

We first discuss INS point-group selection rules in isotropic and anisotropic symmetric spin rings and then turn to a number of polyhedra, which are paradigmatic for spin frustration

TABLE I. Symmetry labels Γ_l specifying $K_{\Gamma_l}(\mathbf{Q})$ functions for unpolarized INS transitions $\Gamma_n \rightarrow \Gamma_m$ in the isotropic D_6 spin ring.^a

	A_1	A_2	B_1	B_2	E_1	E_2
A_1	0	0	B_1	0	E_1	E_2
A_2	0	0	0	B_1	E_1	E_2
B_1	B_1	0	0	0	E_2	E_1
B_2	0	B_1	0	0	E_2	E_1
E_1	E_1	E_1	E_2	E_2	E_2	N/A
E_2	E_2	E_2	E_1	E_1	N/A	E_2

^aThe SPS labels Γ_n and Γ_m of the two different multiplets involved in the transition are given in boldface in the first row and column, respectively. The Γ_l are given in the bulk of the table. An entry 0 means that the transition is forbidden. The N/A entry marks transitions which do not have a uniform \mathbf{Q} dependence [that is, $K_{\Gamma_l}(\mathbf{Q})$ is undefined]. The table is symmetric about the diagonal.

in finite systems and display a number of interesting properties at the classical and quantum levels of description [58]. Chemical synthesis has thus far realized only a subset of these polyhedra in terms of magnetic molecules, and of these only an icosidodecahedral spin cluster was characterized by powder INS (yielding rather broad spectra [59]). However, the present results for INS selection rules and $K_{\Gamma_l}(\mathbf{Q})$ functions should be useful for interpreting possible future experiments on new molecules that may emerge from chemical synthesis.

Spin rings. For D_N spin rings with an even number N of sites, the fundamental basis $\Gamma^{(N)}$ spanned by $\{\hat{s}_i\}$ contains A_1 , B_1 , and every single one of the $(N-2)/2$ different twofold-degenerate E representations exactly once (all Mulliken symmetry labels follow Ref. [53]). For example, $\Gamma^{(4)} = A_1 \oplus B_1 \oplus E$, or $\Gamma^{(6)} = A_1 \oplus B_1 \oplus E_1 \oplus E_2$. A_2 and B_2 are excluded. The ensuing INS selection rules for $N = 6$ can be read from Table I and hold for all D_N spin rings (with even N ; transitions $A \rightarrow A$ or $B \rightarrow B$ are only excluded between different multiplets, see comments above). With the only exception of transitions between different E representations ($E_1 \rightarrow E_2$, or, equivalently, $E_2 \rightarrow E_1$; $I_{nm}(\mathbf{Q})$ is symmetric under an interchange of initial and final states n and m), all transitions have a defined $K_{\Gamma_l}(\mathbf{Q})$. We state without proof that this is true for all even N ; transitions of the type

TABLE II. Coefficients $\bar{c}_t^{\Gamma_l}$ defining $\bar{K}_{\Gamma_l}(Q)$ functions for the isotropic D_6 spin ring. Spin sites are numbered consecutively around the ring.^a

	B_1	E_1	E_2	$n(t)$
(1, 1)	1	1	1	6
(1, 2)	-2	1	-1	12
(1, 3)	2	-1	-1	12
(1, 4)	-1	-1	1	6

^aOne representative site pair (i, j) for each group t of symmetry-equivalent pairs is given in the first column. The $\bar{c}_t^{\Gamma_l}$ are defined in Eq. (18) and are given in the columns headed by a Γ_l symmetry label. The last column lists the number $n(t)$ of pairs in every group, which yields the $c_t^{\Gamma_l}$ coefficients for $K_{\Gamma_l}(\mathbf{Q})$ [Eq. (17)] via $c_t^{\Gamma_l} = \bar{c}_t^{\Gamma_l}/n(t)$. The $n(t)$ always have a common factor of N (the number of sites).

$E_1 \rightarrow E_1$, or $E_2 \rightarrow E_2$, etc., do have a defined $K_{\Gamma_l}(\mathbf{Q})$, where Γ_l is either B_1 , or an E representation.

In order to compactly report the $K_{\Gamma_l}(\mathbf{Q})$ functions, all possible two-index combinations (i, j) are grouped into sets of symmetry-equivalent pairs (formally also counting $i = j$ as a pair). As an example, for a symmetric $N = 4$ ring, there are three types of pairs, which comprise (a) $(i, j) = (1, 1)$, $(2, 2)$, $(3, 3)$, and $(4, 4)$; (b) nearest neighbors, $(i, j) = (1, 2)$, $(2, 3)$, $(3, 4)$, and $(4, 1)$; and (c) next-nearest neighbors, $(i, j) = (1, 3)$ and $(2, 4)$.

In an expansion of $K_{\Gamma_l}(\mathbf{Q})$ in terms of $\cos(\mathbf{Q} \cdot \mathbf{R}_{ij})$,

$$K_{\Gamma_l}(\mathbf{Q}) = \sum_t c_t^{\Gamma_l} \sum_{(i,j) \in t} \cos(\mathbf{Q} \cdot \mathbf{R}_{ij}), \quad (17)$$

t indexes a group of equivalent pairs [$\cos(\mathbf{Q} \cdot \mathbf{R}_{ij}) = \frac{1}{2}(e^{i\mathbf{Q} \cdot \mathbf{R}_{ij}} + e^{i\mathbf{Q} \cdot \mathbf{R}_{ji}}$), cf. Eq. (14)]. This expansion has a total number of N^2 terms, that is, it includes $(i, j) = (1, 2)$ and $(i, j) = (2, 1)$, etc. Equation (17) implicitly defines $K_{\Gamma_l}(\mathbf{Q})$ through the $c_t^{\Gamma_l}$ coefficients.

Upon powder averaging, $\cos(\mathbf{Q} \cdot \mathbf{R}_{ij})$ becomes $j_0(QR_{ij})$. All pairs in a set t have the same $R_{ij} = |\mathbf{R}_{ij}|$. Therefore the expansion for $\bar{K}_{\Gamma_l}(Q)$ (the powder average of $K_{\Gamma_l}(\mathbf{Q})$, up to an

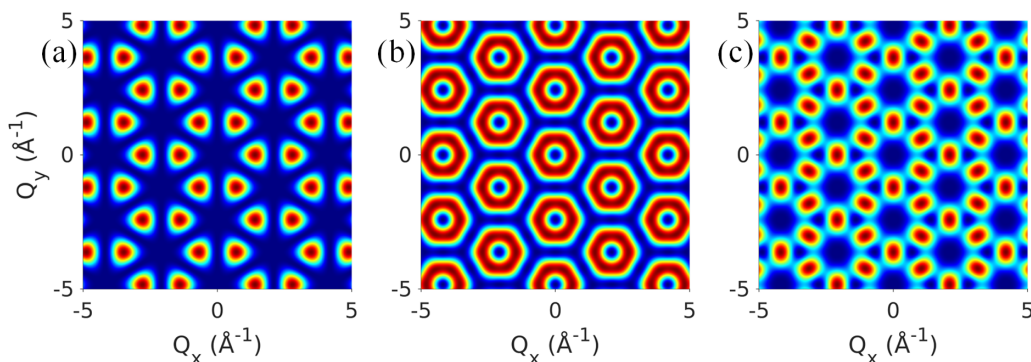


FIG. 1. Single-crystal INS intensity functions $K_{\Gamma_l}(\mathbf{Q})$ for a D_6 spin ring lying in the xy plane, with two spin sites on the x axis. Panels (a), (b), and (c) refer to $\Gamma_l = B_1$, $\Gamma_l = E_1$, and $\Gamma_l = E_2$, respectively. Here and in all other $K_{\Gamma_l}(\mathbf{Q})$ plots in this work, we assume that nearest-neighbor sites are at a distance of $R = 3$ Å. Red color marks high and blue color marks low (zero) intensity. For visibility, the color scales are different for different plots.

TABLE III. Symmetry labels Γ_l specifying $K_{\Gamma_l}(\mathbf{Q})$ functions for unpolarized INS transitions $\Gamma_n \rightarrow \Gamma_m$ in the isotropic D_5 spin ring. For further explanations, see the footnote to Table I.

	A_1	A_2	E_1	E_2
A_1	0	0	E_1	E_2
A_2	0	0	E_1	E_2
E_1	E_1	E_1	E_2	N/A
E_2	E_2	E_2	N/A	E_1

irrelevant constant) contains just a single summation,

$$\bar{K}_{\Gamma_l}(Q) = \sum_t \bar{c}_t^{\Gamma_l} j_0(Qr_t), \quad (18)$$

where r_t is the distance R_{ij} for pairs $(i, j) \in t$. The $\bar{c}_t^{\Gamma_l}$ coefficients are simply related to $c_t^{\Gamma_l}$ through the number $n(t)$ of pairs in t , via $\bar{c}_t^{\Gamma_l} = n(t)c_t^{\Gamma_l}$. Our tables below list only $\bar{c}_t^{\Gamma_l}$ and $n(t)$. For the D_6 spin ring, these quantities are collected in Table II. Each one of the four different pair types is specified in the first column of Table II by one member of each set, specifically, $(i, j) = (1, 1), (1, 2), (1, 3)$, and $(1, 4)$ for $t = 1, 2, 3, 4$.

To avoid any misunderstandings and to illustrate the described instructions for extracting functions $K_{\Gamma_l}(\mathbf{Q})$ and $\bar{K}_{\Gamma_l}(Q)$ from Table II, we exemplarily write them out for $\Gamma_l = B_1$:

$$\begin{aligned} K_{B_1}(\mathbf{Q}) = & 1 - \frac{1}{3}[\cos(\mathbf{Q} \cdot \mathbf{R}_{12}) + \cos(\mathbf{Q} \cdot \mathbf{R}_{23}) + \cos(\mathbf{Q} \cdot \mathbf{R}_{34}) \\ & + \cos(\mathbf{Q} \cdot \mathbf{R}_{45}) + \cos(\mathbf{Q} \cdot \mathbf{R}_{56}) + \cos(\mathbf{Q} \cdot \mathbf{R}_{61})] \\ & + \frac{1}{3}[\cos(\mathbf{Q} \cdot \mathbf{R}_{13}) + \cos(\mathbf{Q} \cdot \mathbf{R}_{24}) + \cos(\mathbf{Q} \cdot \mathbf{R}_{35}) \\ & + \cos(\mathbf{Q} \cdot \mathbf{R}_{46}) + \cos(\mathbf{Q} \cdot \mathbf{R}_{62}) + \cos(\mathbf{Q} \cdot \mathbf{R}_{51})] \\ & - \frac{1}{3}[\cos(\mathbf{Q} \cdot \mathbf{R}_{14}) + \cos(\mathbf{Q} \cdot \mathbf{R}_{25}) + \cos(\mathbf{Q} \cdot \mathbf{R}_{36})] \end{aligned} \quad (19)$$

and

$$\bar{K}_{B_1}(Q) = 1 - 2j_0(R_{12}) + 2j_0(R_{13}) - j_0(R_{14}). \quad (20)$$

A plot of $K_{B_1}(\mathbf{Q})$ [see Fig. 1(a)] was already shown elsewhere [60] (without a group-theoretical analysis, however), but the respective plots of $K_{E_1}(\mathbf{Q})$ and $K_{E_2}(\mathbf{Q})$ [compare Figs. 1(b) and 1(c) to Figs 6(b) and 6(c) in Ref. [60]] are apparently incorrect in the cited work.

We note that the $K_{\Gamma_l}(\mathbf{Q})$ functions can be obtained based on the cyclic group C_N . E representations of D_N fall apart into

TABLE IV. Coefficients $\bar{c}_t^{\Gamma_l}$ defining $\bar{K}_{\Gamma_l}(Q)$ functions for the isotropic D_5 spin ring. Sites are numbered consecutively around the ring. For more explanations, see footnote to Table II.

(i, j)	E_1	E_2	$n(t)$
(1, 1)	2	2	5
(1, 2)	$-1 + \sqrt{5}$	$-1 - \sqrt{5}$	10
(1, 3)	$-1 - \sqrt{5}$	$-1 + \sqrt{5}$	10

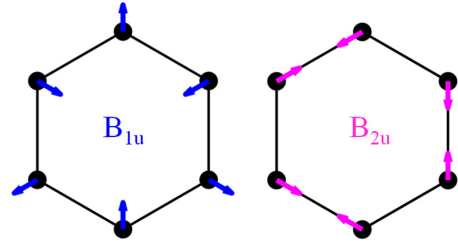


FIG. 2. Symmetry breaking $D_{6h} \rightarrow D_{3h}$ ($D_6 \rightarrow D_3$ for the isotropic spin Hamiltonian) by distorting the structure either along the B_{1u} normal mode (leading to two inequivalent trimers) or along the B_{2u} normal mode (leading to three equivalent dimers).

two “separably degenerate” [61] conjugate representations of C_N , and the individual intensities are added up (see Ref. [32]).

In the context of symmetry breaking, we shall briefly discuss systems that host multiple sets of sites, where point-group operations permute sites only within the separate sets. As a concrete example, we consider two types of $D_6 \rightarrow D_3$ symmetry breaking. For a planar spin ring with D_{6h} molecular symmetry, distortions along the B_{1u} or B_{2u} normal coordinate break symmetry $D_{6h} \rightarrow D_{3h}$ (see Fig. 2), which corresponds to $D_6 \rightarrow D_3$ for the isotropic spin Hamiltonian. Keep in mind, though, that SPS symmetry breaking need not be accompanied by changes in the geometric arrangement of the magnetic ions.

The B_{1u} distortion affords two separate trimers, so the system is partitioned into $n = 2$ sets of $N = 3$ sites each. On the other hand, the B_{2u} distortion leads to dimerization, keeping all six sites equivalent. In the latter case, $\{\hat{s}_i\}$ spans $\Gamma^{(6)} = A_1 \oplus A_2 \oplus 2E$, so INS transitions $A_1 \rightarrow A_1$ and $A_2 \rightarrow A_2$ are forbidden. On the other hand, distortions in D_{2N} spin rings, $D_{2N} \rightarrow D_N$, which produce $n = 2$ sets with N members each (this obtains for the B_{1u} distortion in the foregoing $D_6 \rightarrow D_3$ example), will simply double all representations compared to an N -site D_N system. For example, $\{\hat{s}_i\}$ spans $\Gamma^{(6)} = 2(A_1 \oplus E) = 2A_1 + 2E$ for $D_6 \rightarrow D_3$, or $\Gamma^{(12)} = 2(A_1 \oplus B_1 \oplus E_1 \oplus E_2)$ for $D_{12} \rightarrow D_6$, etc. Thus, the same INS selection rules valid for N -site D_N systems still hold, but \mathbf{Q} dependencies are not uniquely defined by symmetry, because all representations occur multiple times. There is, however, one exception to the latter statement on selection

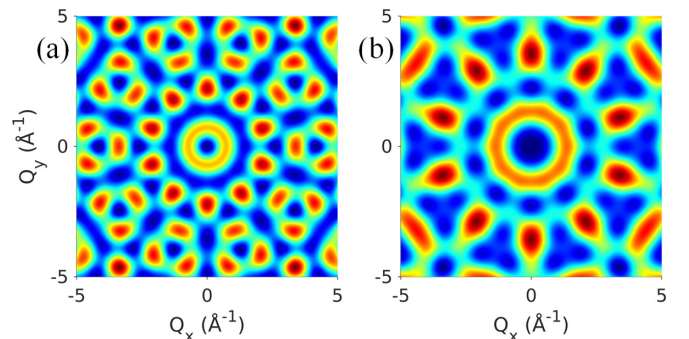


FIG. 3. Single-crystal INS intensity functions $K_{\Gamma_l}(\mathbf{Q})$ for a D_5 spin ring lying in the xy plane, with one site on the x axis. Panels (a) and (b) refer to $\Gamma_l = E_1$ and $\Gamma_l = E_2$, respectively.

TABLE V. Isomorphism between generators of the real-space D_{6h} point group (left column) and symmetry operations of the corresponding anisotropic spin Hamiltonian (right column).^a

C_6	$\hat{P}_{12}\hat{P}_{23}\hat{P}_{34}\hat{P}_{45}\hat{P}_{56} \times \exp(-i\frac{2\pi}{6}\hat{S}_z)$
C_2	$\hat{P}_{16}\hat{P}_{25}\hat{P}_{34} \times \exp(-i\pi\hat{S}_y)$
C_i	$\hat{P}_{14}\hat{P}_{25}\hat{P}_{36}$

^aSites are numbered consecutively around the ring. The ring lies in the xy plane, with two sites on the x axis. A permutation that corresponds to a real-space rotation about some axis by angle ϕ must be combined with a spin rotation about that same axis, but by the opposite angle $(-\phi)$, in order to represent a symmetry of the anisotropic Hamiltonian [39].

rules and \mathbf{Q} dependencies, because now two orthogonal A_1 operators can be formed: the total-spin operator, Eq. (9), which cannot cause transitions between different multiplets, and a Néel-type vector operator,

$$\hat{\mathbf{T}}_{A_1} = \sum_i (-1)^i \hat{\mathbf{s}}_i, \quad (21)$$

where sites in the first and second set have odd and even numbers, respectively. Thus, transitions between multiplets that transform as the same one-dimensional representation become allowed, and they have a universal \mathbf{Q} dependence because there is only one transition operator, Eq. (21). The \mathbf{Q} -dependent function for such transitions is given in Eq. (22),

$$K_{A_1}(\mathbf{Q}) = \sum_{i,j} e^{i\mathbf{Q}\cdot\mathbf{R}_{ij}} (-1)^{i+j}, \quad (22)$$

which is the same functional form as $K_{B_1}(\mathbf{Q})$ in the symmetrical D_{2N} system (or $K_B(\mathbf{Q})$ in C_{2N}). More generally, in systems with D_N symmetry, with n sets of N sites, the above-specified general selection rules are valid. For example, for the Mn_{12} single-molecule magnet with S_4 molecular symmetry, it is a good approximation to regard a Heisenberg model with D_4 -SPS [30], so there are $n = 3$ sets of $N = 4$ equivalent centers. Selection rules arise from the fact that A_2 and B_2 are excluded from $\Gamma^{(12)} = 3(A_1 \oplus B_1 \oplus E)$. As A_1 occurs

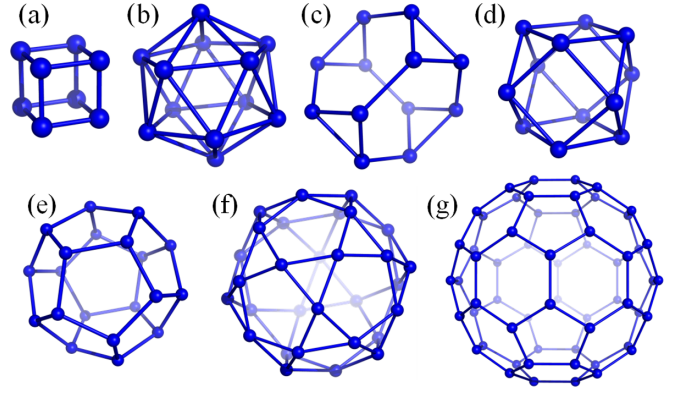


FIG. 4. Polyhedra studied in the present work. A spin is positioned at every vertex (marked by spheres): (a) cube, (b) icosahedron, (c) truncated tetrahedron, (d) cuboctahedron, (e) dodecahedron, (f) icosidodecahedron, and (g) truncated icosahedron. Pictures of the polyhedra were generated with the PYMOL software.

three times, transitions $A_1 \rightarrow A_1$, $A_2 \rightarrow A_2$, $B_1 \rightarrow B_1$, or $B_2 \rightarrow B_2$ can be mediated by two different $\hat{\mathbf{T}}_{A_1}$ operators, and there is consequently no universal $K_{A_1}(\mathbf{Q})$ function. In other words, there is no universal \mathbf{Q} dependence, even when neglecting differences in form factors between different types of ions. In later sections we address additional consequences of symmetry breaking for the cube and the icosahedron.

As a general point it is worth mentioning that transitions may be excluded for certain directions of \mathbf{Q} . Expressing $I_{nm}(\mathbf{Q})$ of Eq. (5) in terms of $\hat{\mathbf{V}} = \sum_i e^{-i\mathbf{Q}\cdot\mathbf{R}_i} \hat{\mathbf{s}}_i$ and assuming a uniform form factor for all ions yields Eq. (23),

$$I_{nm}(\mathbf{Q}) = |F(Q)|^2 \sum_{\alpha,\beta} \left(\delta_{\alpha\beta} - \frac{Q_\alpha Q_\beta}{Q^2} \right) \langle n | \hat{V}_\alpha^\dagger | m \rangle \langle m | \hat{V}_\beta | n \rangle. \quad (23)$$

For a planar molecule, $\hat{\mathbf{V}} = \hat{\mathbf{S}}$ if \mathbf{Q} is perpendicular to the plane, leading to $I_{nm}(\mathbf{Q}) = 0$. In a sense, this is another combined spin- and point-group selection rule, although the geometrical planarity of the molecule does not show up in the isotropic spin Hamiltonian.

TABLE VI. Decompositions of the fundamental representations $\Gamma^{(N)}$ and $\Gamma^{(3N)}$ for SPS or permutational-rotational symmetry groups of isotropic and anisotropic spin models, respectively, for the spin polyhedra considered in this work. Mulliken symmetry labels follow Ref. [53].

System	N	Group	$\Gamma^{(N)}$	$\Gamma^{(3N)}$
Cube	8	O_h	$A_{1g} \oplus A_{2u} \oplus T_{1u} \oplus T_{2g}$	$A_{1u} \oplus A_{2g} \oplus E_g \oplus E_u \oplus 2T_{1g} \oplus T_{1u} \oplus T_{2g} \oplus 2T_{2u}$
Icosahedron	12	I_h	$A_g \oplus T_{1u} \oplus T_{2u} \oplus H_g$	$A_u \oplus 2T_{1g} \oplus T_{1u} \oplus T_{2g} \oplus F_g \oplus F_u \oplus H_g \oplus 2H_u$
Truncated tetrahedron	12	T_d	$A_1 \oplus E \oplus T_1 \oplus 2T_2$	$A_1 \oplus 2A_2 \oplus 3E \oplus 5T_1 \oplus 4T_2$
Cuboctahedron	12	O_h	$A_{1g} \oplus E_g \oplus T_{1u} \oplus T_{2g} \oplus T_{2u}$	$A_{1u} \oplus A_{2g} \oplus A_{2u} \oplus E_g \oplus 2E_u \oplus 3T_{1g} \oplus 2T_{1u} \oplus 2T_{2g} \oplus 2T_{2u}$
Dodecahedron	20	I_h	$A_g \oplus T_{1u} \oplus T_{2u} \oplus F_g \oplus F_u \oplus H_g$	$A_u \oplus 2T_{1g} \oplus T_{1u} \oplus 2T_{2g} \oplus T_{2u} \oplus 2F_g \oplus 2F_u \oplus 2H_g \oplus 3H_u$
Icosidodecahedron	30	I_h	$A_g \oplus T_{1u} \oplus T_{2u} \oplus F_g \oplus F_u \oplus 2H_g \oplus H_u$	$A_u \oplus 3T_{1g} \oplus 2T_{1u} \oplus 3T_{2g} \oplus 2T_{2u} \oplus 3F_g \oplus 3F_u \oplus 3H_g \oplus 4H_u$
Truncated icosahedron	60	I_h	$A_g \oplus T_{1g} \oplus 2T_{1u} \oplus T_{2g} \oplus 2T_{2u} \oplus 2F_g \oplus 2F_u \oplus 3H_g \oplus 2H_u$	$A_g \oplus 2A_u \oplus 5T_{1g} \oplus 4T_{1u} \oplus 5T_{2g} \oplus 4T_{2u} \oplus 6F_g \oplus 6F_u \oplus 7H_g \oplus 8H_u$

TABLE VII. O_h symmetry labels Γ_l specifying $K_{\Gamma_l}(\mathbf{Q})$ functions for unpolarized INS transitions $\Gamma_n \rightarrow \Gamma_m$ in the isotropic spin cube. For further explanations, see the footnote to Table I.

	A_{1g}	A_{2g}	E_g	T_{1g}	T_{2g}	A_{1u}	A_{2u}	E_u	T_{1u}	T_{2u}
A_{1g}	0	0	0	0	T_{2g}	0	A_{2u}	0	T_{1u}	0
A_{2g}	0	0	0	T_{2g}	0	A_{2u}	0	0	0	T_{1u}
E_g	0	0	0	T_{2g}	T_{2g}	0	0	A_{2u}	T_{1u}	T_{1u}
T_{1g}	0	T_{2g}	T_{2g}	T_{2g}	T_{2g}	T_{1u}	0	T_{1u}	T_{1u}	N/A
T_{2g}	T_{2g}	0	T_{2g}	T_{2g}	T_{2g}	0	T_{1u}	T_{1u}	N/A	T_{1u}
A_{1u}	0	A_{2u}	0	T_{1u}	0	0	0	0	0	T_{2g}
A_{2u}	A_{2u}	0	0	0	T_{1u}	0	0	0	0	T_{2g}
E_u	0	0	A_{2u}	T_{1u}	T_{1u}	0	0	0	T_{2g}	T_{2g}
T_{1u}	T_{1u}	0	T_{1u}	T_{1u}	N/A	0	T_{2g}	T_{2g}	T_{2g}	T_{2g}
T_{2u}	0	T_{1u}	T_{1u}	N/A	T_{1u}	T_{2g}	0	T_{2g}	T_{2g}	T_{2g}

For D_N spin rings with odd N , $\Gamma^{(N)}$ spans A_1 and all $(N-1)/2$ different E representations exactly once, with A_2 excluded. For example, $\Gamma^{(5)} = A_1 \oplus E_1 \oplus E_2$, or $\Gamma^{(7)} = A_1 \oplus E_1 \oplus E_2 \oplus E_3$. The resulting selection rules for D_5 can be read from Table III. Just like for even N , all types of transitions, except those between multiplets belonging to different E representations, have a defined $K_{\Gamma_l}(\mathbf{Q})$, see Table IV. This is indeed a property holding for all $N \geq 3$.

The $K_{\Gamma_l}(\mathbf{Q})$ functions are inversion symmetric, $K_{\Gamma_l}(\mathbf{Q}) = K_{\Gamma_l}(-\mathbf{Q})$. Therefore, in the D_5 ring, each $K_{\Gamma_l}(\mathbf{Q})$ has symmetry $D_5 \times C_i = D_{5d}$ in \mathbf{Q} space. This manifests as a tenfold rotational symmetry in the Q_x, Q_y plane, see Fig. 3.

We next discuss anisotropic spin rings based on groups D_N or D_{Nh} . For D_{6h} , the isomorphism between the group generators of the real-space symmetry group and the respective symmetry group of the anisotropic spin Hamiltonian is given in Table V.

The permutation operator corresponding to a C_6 rotation can be written as a product of overlapping interchanges, $\hat{P}_{123456} = \hat{P}_{12}\hat{P}_{23}\hat{P}_{34}\hat{P}_{45}\hat{P}_{56}$. [For $s = \frac{1}{2}$, $\hat{P}_{ij} = \frac{1}{2}(1 + 4\hat{s}_i \cdot \hat{s}_j)$ [62].] In an uncoupled spin basis, \hat{P}_{123456} effects a cyclic shift in the \hat{s}_{iz} eigenvalues m_i ,

$$\hat{P}_{123456}|m_1, m_2, m_3, m_4, m_5, m_6\rangle = |m_6, m_1, m_2, m_3, m_4, m_5\rangle. \quad (24)$$

In an isotropic model for a molecule with D_{6h} symmetry, real-space operations C_6^3 and C_i correspond to the same SPS operation, so the isotropic spin Hamiltonian can be said to have only D_6 SPS symmetry (and full spin-rotational symmetry). However, in the anisotropic case, the operations corresponding to C_6^3 and C_i differ by a spin rotation by an-

TABLE VIII. Coefficients $\bar{c}_i^{\Gamma_l}$ defining $\bar{K}_{\Gamma_l}(\mathbf{Q})$ functions for the isotropic spin cube. Site numbers are defined in Fig. 5. For more explanations, see the footnote to Table II.

	A_{2u}	T_{1u}	T_{2g}	$n(t)$
(1, 1)	1	1	1	8
(1, 2)	-3	1	-1	24
(1, 3)	3	-1	-1	24
(1, 4)	-1	-1	1	8

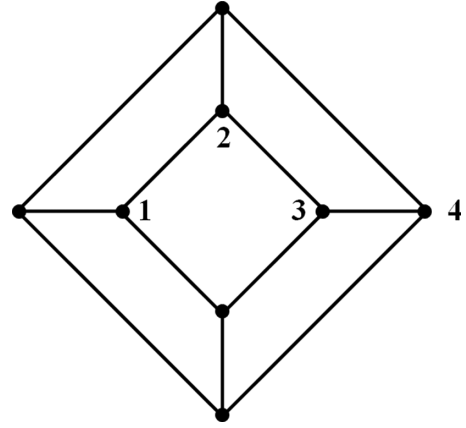


FIG. 5. Schlegel diagram for the cube, where only those sites are numbered which form inequivalent pairs with site 1.

gle π about the z axis. This also implies that spin-rotational symmetry is not completely broken, because the anisotropic Hamiltonian is invariant under $\exp(-i\pi\hat{S}_z)$.

Taking an anisotropic $s = \frac{1}{2}$ ring with D_{6h} symmetry as an example, the decomposition of the basis of $2^6 = 64$ states in terms of irreducible representations is given in Eq. (25):

$$\Gamma^{(64)} = A_{1g} \oplus 2A_{1u} \oplus 5A_{2g} \oplus 2A_{2u} \oplus 4B_{1g} \oplus 5B_{2g} \oplus 4B_{2g} \oplus B_{2u} \oplus 6E_{1g} \oplus 5E_{1u} \oplus 5E_{2g} \oplus 4E_{2u} \quad (25)$$

We briefly comment on the similarity between a symmetry analysis of the combined translational (3), rotational (3), and vibrational $(3N-6)$ degrees of freedom spanned by the position vectors $\{\mathbf{R}_i\}$ [51] and the respective problem for $\{\hat{s}_i\}$. For operations corresponding to proper real-space rotations, $\{\mathbf{R}_i\}$ and $\{\hat{s}_i\}$ transform isomorphically, but this is not true for improper rotations. As an example, the inversion operation C_i effects a permutation among the $\{\mathbf{R}_i\}$ and inverts all local axis systems (overall, $\mathbf{R}_i \rightarrow -\mathbf{R}_i$), while the $\{\hat{s}_i\}$ are only permuted (that is, $\hat{s}_i \rightarrow \hat{s}_j$, cf. Table V).

In an anisotropic D_6 ring, $\Gamma^{(18)}$ spanned by $\{\hat{s}_i\}$ includes all representations at least once, $\Gamma^{(18)} = A_1 \oplus 2A_2 \oplus B_1 \oplus 2B_2 \oplus 3E_1 \oplus 3E_2$. Therefore no INS selection rules are expected. However, in D_{6h} , A_{1g} and B_{1u} are missing,

$$\Gamma^{(18)} = A_{1u} \oplus A_{2g} \oplus A_{2u} \oplus B_{1g} \oplus B_{2g} \oplus B_{2u} \oplus 2E_{1g} \oplus E_{1u} \oplus E_{2g} \oplus 2E_{2u}. \quad (26)$$

Thus some transitions are forbidden (e.g., $A_{1g} \rightarrow A_{1g}$ or $A_{1g} \rightarrow B_{1u}$), with analogous relations for other D_{Nh} systems (with N even). In the D_5 ring, all representations are included in $\Gamma^{(15)} = A_1 \oplus 2A_2 \oplus 3E_1 \oplus 3E_2$, precluding selection rules. We shall not specifically discuss odd-spin systems (for rings, this obtains for odd N and $s = \frac{1}{2}, \frac{3}{2}, \dots$) but note that Γ_n and Γ_m would then refer to fermionic representations of the respective double group, while $\Gamma^{(3N)}$ is still decomposed in terms of bosonic representations. As usual, a transition $\Gamma_n \rightarrow \Gamma_m$ is forbidden if $\Gamma_n^* \times \Gamma^{(3N)} \times \Gamma_m$ does not contain Γ_1 .

Lastly, for anisotropic rings lying in the xy plane, we have $\hat{\mathbf{V}} = \hat{\mathbf{S}}$, when $\mathbf{Q} = (0, 0, \pm Q)^T$, as explained [see Eq. (23)]. To determine if a transition with momentum transfer perpen-

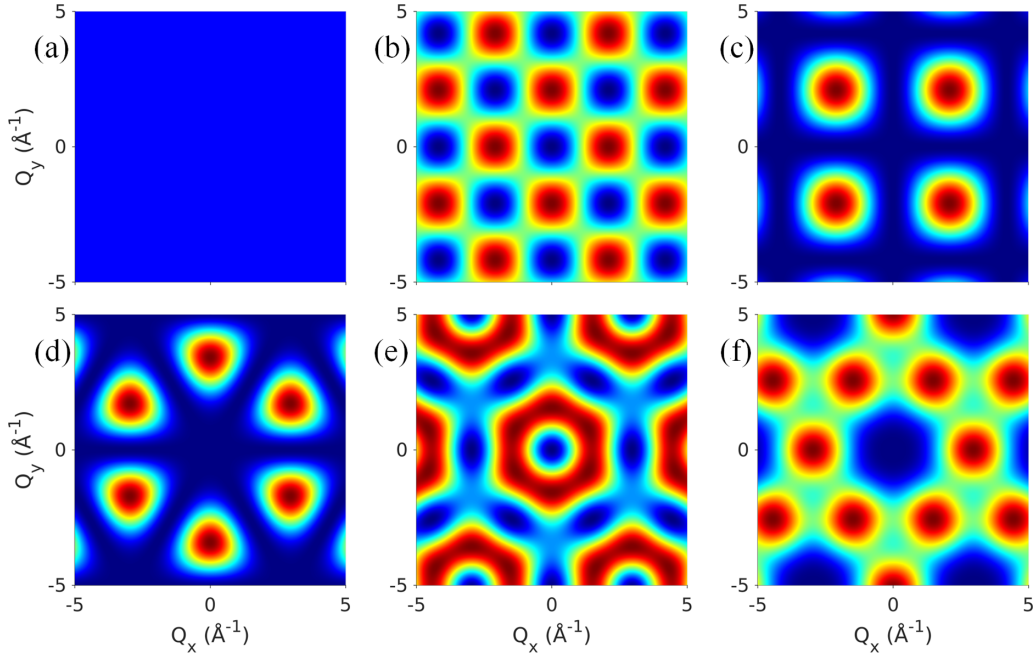


FIG. 6. Single-crystal INS intensity functions $K_{\Gamma_l}(\mathbf{Q})$ in a spin cube. First row (panels (a)–(c)): C_4 axis oriented along z , site coordinates $(\pm 1.5, \pm 1.5, \pm 1.5)\text{\AA}$. Second row [(d)–(f)]: C_3 axis oriented along z , and yz is a mirror plane of the cube. The Γ_l labels are A_{2u} [(a), (d)], T_{1u} [(b), (e)], and T_{2g} [(c), (f)]. In panel (a), $K_{A_{2u}}(\mathbf{Q}) = 0$.

pendicular to the ring plane is allowed, we must determine how $\hat{\mathbf{S}}$ transforms in the rotational-permutational symmetry group ($\hat{\mathbf{S}}$ is symmetric under all permutations). In D_{Nh} ($N \geq 3$), $\hat{\mathbf{S}}$ transforms as $A_{2g} \oplus E_{1g}$ for even N and as $A'_2 \oplus E''_1$ for odd N , and the resulting selection rules are easily derived. A more general discussion of how INS intensities can vanish for specific \mathbf{Q} is beyond the scope of this work.

Spin polyhedra. The polyhedra that are discussed here are shown in Fig. 4. The fundamental representations $\Gamma^{(N)}$ and $\Gamma^{(3N)}$ spanned by the set $\{\hat{\mathbf{s}}_i\}$ in the groups relevant for isotropic and anisotropic spin Hamiltonians, respectively, are collected in Table VI.

The decompositions of $\Gamma^{(N)}$ and $\Gamma^{(3N)}$ were independently calculated here, but for several (perhaps all) of the considered polyhedra, the $\Gamma^{(N)}$ decompositions were reported elsewhere (see, e.g., Refs. [40,63,64]; symmetry labels in Ref. [63] did

TABLE IX. I_h symmetry labels Γ_l specifying $K_{\Gamma_l}(\mathbf{Q})$ functions for unpolarized INS transitions $\Gamma_n \rightarrow \Gamma_m$ in the isotropic spin icosahedron. For further explanations, see the footnote to Table I.

	A_g	T_{1g}	T_{2g}	F_g	H_g	A_u	T_{1u}	T_{2u}	F_u	H_u
A_g	0	0	0	0	H_g	0	T_{1u}	T_{2u}	0	0
T_{1g}	0	H_g	H_g	H_g	H_g	T_{1u}	T_{1u}	0	T_{2u}	N/A
T_{2g}	0	H_g	H_g	H_g	H_g	T_{2u}	0	T_{2u}	T_{1u}	N/A
F_g	0	H_g	H_g	H_g	H_g	0	T_{2u}	T_{1u}	N/A	N/A
H_g	H_g	H_g	H_g	H_g	H_g	0	N/A	N/A	N/A	N/A
A_u	0	T_{1u}	T_{2u}	0	0	0	0	0	0	H_g
T_{1u}	T_{1u}	T_{1u}	0	T_{2u}	N/A	0	H_g	H_g	H_g	H_g
T_{2u}	T_{2u}	0	T_{2u}	T_{1u}	N/A	0	H_g	H_g	H_g	H_g
F_u	0	T_{2u}	T_{1u}	N/A	N/A	0	H_g	H_g	H_g	H_g
H_u	0	N/A	N/A	N/A	N/A	H_g	H_g	H_g	H_g	H_g

not include the C_i operation in groups $I_h = I \times C_i$ or $O_h = O \times C_i$). Besides, decompositions of $\Gamma^{(3N)}$ could be easily deduced from information on the symmetries of vibrational normal modes (where available). Take the truncated icosahedron as an example, most famously realized in the C_{60} fullerene. In the group $I_h = I \times C_i$, $\{\mathbf{R}_i\}$ and $\{\hat{\mathbf{s}}_i\}$ transform isomorphically with respect to I , but oppositely under C_i (see comments above). Separating the translational and rotational degrees of freedom (T_{1g} and T_{1u}) from $\Gamma^{(180)}$ (last entry in Table VI) and switching parity ($g \rightarrow u, u \rightarrow g$) yields the symmetry decomposition for vibrational normal modes in C_{60} [65].

We shall list our results for the INS \mathbf{Q} dependencies for these systems in the order of their appearance in Table VI. We plot all $K_{\Gamma_l}(\mathbf{Q})$ in $Q_z = 0$ planes in \mathbf{Q} space that are perpendicular to a threefold, fourfold, or fivefold symmetry axis (where the symmetry axis is defined as the z axis). In the former two cases, the plots have sixfold and fourfold rotational symmetry, as well as translational symmetry. In planes perpendicular to a fivefold axis, $K_{\Gamma_l}(\mathbf{Q})$ has tenfold rotational symmetry (see comments above) and it is quasiperiodic under translations. For portraying the $K_{\Gamma_l}(\mathbf{Q})$ functions in plots, we chose larger

TABLE X. Coefficients $\bar{c}_i^{\Gamma_l}$ defining $\bar{K}_{\Gamma_l}(\mathbf{Q})$ functions for the isotropic spin icosahedron. Site numbers are defined in Fig. 7. For more explanations, see footnote to Table II.

	T_{1u}	T_{2u}	H_g	$n(t)$
(1, 1)	1	1	1	12
(1, 2)	$\sqrt{5}$	$-\sqrt{5}$	-1	60
(1, 3)	$-\sqrt{5}$	$\sqrt{5}$	-1	60
(1, 4)	-1	-1	1	12

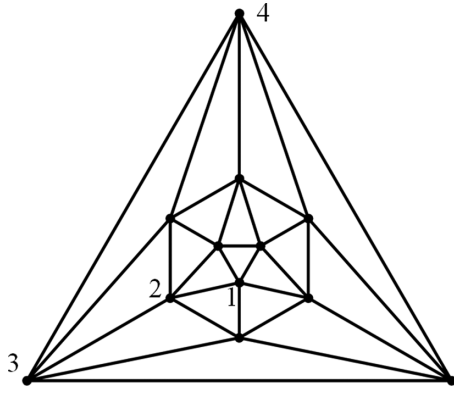


FIG. 7. Schlegel diagram for the icosahedron. Only those sites are numbered which form inequivalent pairs with site 1.

ranges in \mathbf{Q} space than for the spin rings (keeping the internuclear distance at a more or less representative value of $R = 3 \text{ \AA}$), even though intensities of magnetic transitions with such large Q may be difficult (or impossible, due to kinematic constraints) to observe with current INS facilities. However, in several cases our plot range in the Q_x, Q_y plane is still not large enough to display the periodicity or quasiperiodicity.

Cube. Pseudocubic spin clusters of mixed-metal [66], localized mixed-valence [67], and uniform-valence [68] type were reported (however, in the latter case [68], the ligands bridging a cubic core of eight Co^{2+} ions break cubic symmetry). To the best of our knowledge, no symmetric cubes, where all eight spin sites are equivalent, were obtained yet.

The general structure of reporting the $K_{\Gamma_l}(\mathbf{Q})$ functions comprises two tables and two figures. First, Table VII contains information on Γ_l as a function of $\Gamma_n \rightarrow \Gamma_m$, as well as information on forbidden transitions and those that do not have a

TABLE XI. T_d symmetry labels Γ_l specifying $K_{\Gamma_l}(\mathbf{Q})$ functions for unpolarized INS transitions $\Gamma_n \rightarrow \Gamma_m$ in the isotropic truncated tetrahedron. For further explanations, see the footnote to Table I.

	A_1	A_2	E	T_1	T_2
A_1	0	0	E	T_1	N/A
A_2	0	0	E	N/A	T_1
E	E	E	E	N/A	N/A
T_1	T_1	N/A	N/A	N/A	N/A
T_2	N/A	T_1	N/A	N/A	N/A

defined $K_{\Gamma_l}(\mathbf{Q})$. Second, the coefficients $c_t^{\Gamma_l}$ [see Eq. (18)], the number $n(t)$ of pairs in each group t , and one representative pair defining each group t are collected in Table VIII. The numbering of sites is defined in a Schlegel diagram drawn in Fig. 5, and the $K_{\Gamma_l}(\mathbf{Q})$ are finally plotted in two different planes in \mathbf{Q} space in Fig. 6.

Interestingly, under certain conditions $K_{\Gamma_l}(\mathbf{Q})$ functions, or, more frequently, their powder averages $\bar{K}_{\Gamma_l}(Q)$, still apply to systems with lower SPS symmetry. To illustrate this point, we consider $O_h \rightarrow D_4$ SPS symmetry breaking in the cube, whereupon the representations occurring in $\Gamma^{(8)} = A_{1g} \oplus A_{2u} \oplus T_{1u} \oplus T_{2g}$ (cf. Table VI) become $A_{1g} \rightarrow A_1$, $A_{2u} \rightarrow B_1$, $T_{1u} \rightarrow A_2 \oplus E$, and $T_{2g} \rightarrow B_2 \oplus E$, yielding overall

$$\Gamma^{(8)} = A_1 \oplus B_1 \oplus A_2 \oplus B_2 \oplus 2E. \quad (27)$$

Then, for transitions between one-dimensional representations of D_4 that are mediated by \hat{T}_{B_1} , the universal $K_{B_1}(\mathbf{Q})$ function for the D_4 system is the same as $K_{A_{2u}}(\mathbf{Q})$ in the O_h system, to the degree that deviations from a geometrical O_h structure can be neglected. As the A_2 and B_2 transition operators in the D_4 system originate from a single component of T_{1u} and T_{2g} , respectively, the single-crystal functions $K_{A_2}(\mathbf{Q})$ and $K_{B_2}(\mathbf{Q})$ are different from $K_{T_{1u}}(\mathbf{Q})$ and $K_{T_{2g}}(\mathbf{Q})$, because each

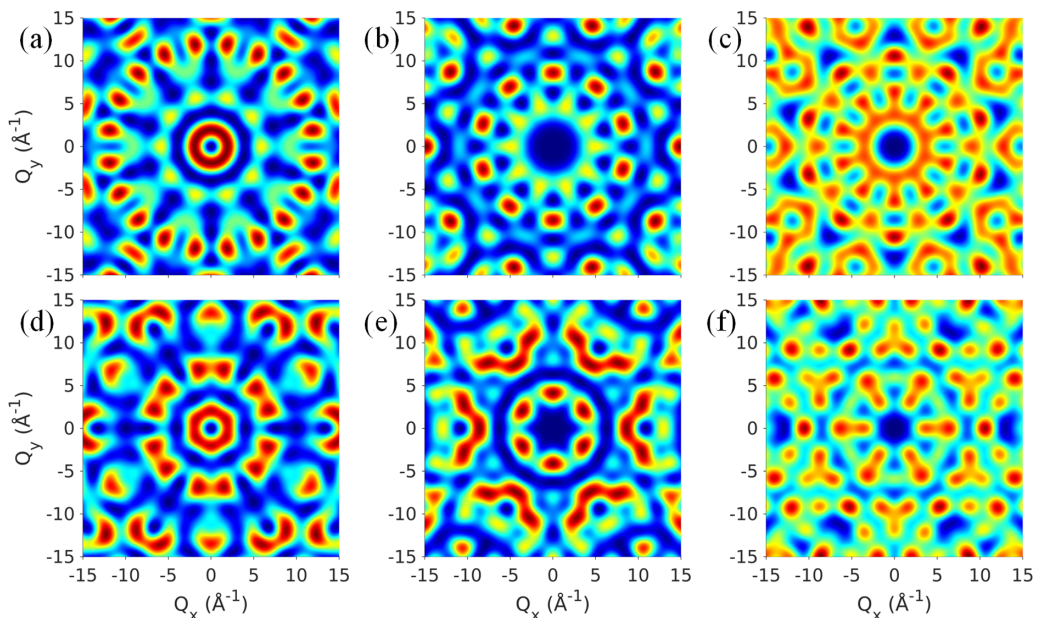


FIG. 8. $K_{\Gamma_l}(\mathbf{Q})$ functions for the icosahedron. First row [(a)–(c)]: C_5 axis oriented along z . Second row [(d)–(f)]: C_3 axis oriented along z . In all cases, yz is a mirror plane of the icosahedron. The Γ_l label is T_{1u} [(a), (d)], T_{2u} [(b), (e)], or H_g [(c), (f)].

TABLE XII. Coefficients $\bar{c}_i^{\Gamma_l}$ defining $\bar{K}_{\Gamma_l}(\mathbf{Q})$ functions for the isotropic truncated tetrahedron.^a Site numbers are defined in Fig. 9. For more explanations, see footnote to Table II.

	T ₁	E	T ₂ (I)	T ₂ (II)	$n(t)$
(1, 1)	1	1	3	3	12
(1, 2)	-1	-1	-2	5	24
(1, 3)	-1	1	-1	1	12
(1, 4)	2	-2	-4	-2	48
(1, 5)	-1	-1	6	-3	24
(1, 6)	0	2	2	-4	24

^aThe entries for T₂(I) and T₂(II) refer to FCSWT transitions, with adjacency-matrix eigenvalues of $J[\text{T}_2(\text{I})] = -1$ and $J[\text{T}_2(\text{II})] = 2$, respectively, see main text.

of the latter results from summing over all three components. However, the powder averages $\bar{K}_{A_2}(\mathbf{Q})$ and $\bar{K}_{B_2}(\mathbf{Q})$ are the same as $\bar{K}_{T_{1u}}(\mathbf{Q})$ and $\bar{K}_{T_{1u}}(\mathbf{Q})$, respectively (again, assuming that the geometrical structure remains a perfect cube). Another example of symmetry breaking is discussed for the icosahedron in the following section.

An anisotropic spin Hamiltonian for the cube with NN couplings [Eqs. (2) and (3)] has an artificially high symmetry, because certain spin rotations and permutations are separate symmetries, affording a complicated group of order $h = 1152$. The symmetry is reduced to O_h when anisotropic couplings between other sites (beyond nearest neighbors) are included. Only A_{1g} is excluded from $\Gamma^{(24)}$ (cf. Table VI). Therefore only transitions $A_{1g} \rightarrow A_{1g}$, $A_{1u} \rightarrow A_{1u}$, $A_{2g} \rightarrow A_{2g}$, and $A_{2u} \rightarrow A_{2u}$ are forbidden in a general anisotropic spin cube.

Icosahedron. An unusual first-order field-dependent magnetization discontinuity in the classical Heisenberg icosahedron [69] indicates a large jump in the magnetization quantum number in a quantum-mechanical treatment for large values of s [41,69]. Similar effects had been detected in the dodecahedron and the truncated icosahedron [70] and were later studied in more detail [71]. Somewhat unfortunately, intense efforts to synthesize an icosahedral spin cluster were not successful but yielded an $\{\text{Fe}_9\}$ species composed of Fe^{3+} ($s = \frac{5}{2}$) ions, corresponding to a tridiminished icosahedron [72]. This molecule was studied by INS [73,74]. It is certainly not excluded that

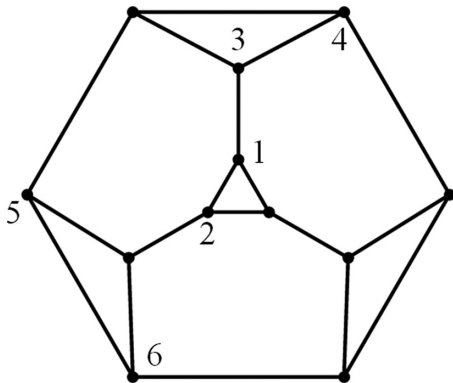


FIG. 9. Schlegel diagram for the truncated tetrahedron, where only those sites are numbered which form inequivalent pairs with site 1.

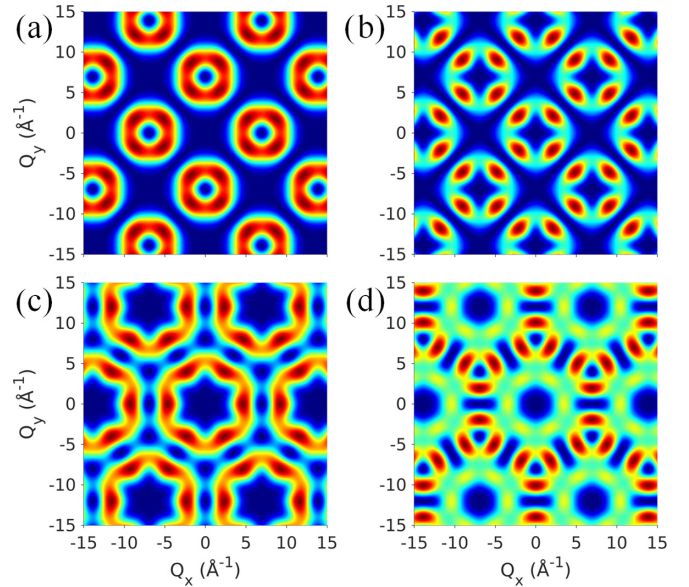


FIG. 10. $K_{\Gamma_l}(\mathbf{Q})$ functions for the truncated tetrahedron. First row [(a), (b)]: S_4 axis oriented along z . Second row [(c), (d)]: C_3 axis oriented along z . In all cases, yz is a mirror plane of the truncated tetrahedron. The Γ_l label is T₁ [(a), (c)] or E [(b), (d)].

genuine spin icosahedra will exist at a later time. The information on \mathbf{Q} dependencies is altogether contained in Table IX, Table X, Fig. 7, and Fig. 8.

As another example for the consequences of SPS symmetry breaking, we consider $I_h \rightarrow D_{5d}$ (e.g., by stretching or contracting the icosahedron along a C_5 axis). Upon symmetry descent, $T_{1u} \rightarrow A_{2u} \oplus E_{1u}$, $T_{2u} \rightarrow A_{2u} \oplus E_{2u}$, and $H_g \rightarrow A_{1g} \oplus E_{1g} \oplus E_{2g}$, and we overall obtain

$$\Gamma^{(12)} = 2A_{1g} \oplus 2A_{2u} \oplus E_{1g} \oplus E_{2g} \oplus E_{1u} \oplus E_{2u}. \quad (28)$$

In addition to the trivial total-spin operator [Eq. (9)], there is a second $\Gamma_1 = A_{1g}$ operator in $\Gamma^{(12)}$,

$$\hat{T}_{A_{1g}} = 5(\hat{s}_1 + \hat{s}_4) - \sum_{i \neq 1,4} \hat{s}_i, \quad (29)$$

where sites on the C_5 axis have numbers 1 and 4. This operator [Eq. (29)] transforms as a single component of H_g

TABLE XIII. O_h symmetry labels Γ_l specifying $K_{\Gamma_l}(\mathbf{Q})$ functions for unpolarized INS transitions $\Gamma_n \rightarrow \Gamma_m$ in the isotropic cuboctahedron. For further explanations, see the footnote to Table I.

	A_{1g}	A_{2g}	E_g	T_{1g}	T_{2g}	A_{1u}	A_{2u}	E_u	T_{1u}	T_{2u}
A_{1g}	0	0	E_g	0	T_{2g}	0	0	0	T_{1u}	T_{2u}
A_{2g}	0	0	E_g	T_{2g}	0	0	0	0	T_{2u}	T_{1u}
E_g	E_g	E_g	E_g	T_{2g}	T_{2g}	0	0	0	N/A	N/A
T_{1g}	0	T_{2g}	T_{2g}	N/A	N/A	T_{1u}	T_{2u}	N/A	N/A	N/A
T_{2g}	T_{2g}	0	T_{2g}	N/A	N/A	T_{2u}	T_{1u}	N/A	N/A	N/A
A_{1u}	0	0	0	T_{1u}	T_{2u}	0	0	E_g	0	T_{2g}
A_{2u}	0	0	0	T_{2u}	T_{1u}	0	0	E_g	T_{2g}	0
E_u	0	0	0	N/A	N/A	E_g	E_g	E_g	T_{2g}	T_{2g}
T_{1u}	T_{1u}	T_{2u}	N/A	N/A	N/A	0	T_{2g}	T_{2g}	N/A	N/A
T_{2u}	T_{2u}	T_{1u}	N/A	N/A	N/A	T_{2g}	0	T_{2g}	N/A	N/A

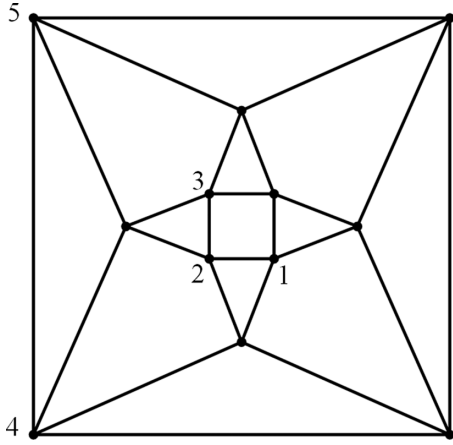


FIG. 11. Schlegel diagram for the cuboctahedron. Only sites forming inequivalent pairs with site 1 are numbered.

in I_h . While $K_{A_{1g}}(\mathbf{Q})$ in D_{5d} is different from $K_{H_g}(\mathbf{Q})$ in I_h , because $K_{H_g}(\mathbf{Q})$ is obtained by summing over all five components of H_g , the powder average $\bar{K}_{A_{1g}}(Q)$ in the D_{5d} system is the same as $\bar{K}_{H_g}(Q)$ in the I_h system (to the degree that changes in the geometrical structure can be neglected), and $\bar{K}_{A_{1g}}(Q) = \bar{K}_{E_{1g}}(Q) = \bar{K}_{E_{2g}}(Q)$. By the same reasoning, $\bar{K}_{E_{1u}}(Q)$ and $\bar{K}_{E_{2u}}(Q)$ in D_{5d} agree with $\bar{K}_{T_{1u}}(Q)$ and $\bar{K}_{T_{2u}}(Q)$ in I_h , respectively. We refrain from discussing symmetry breaking for other polyhedral clusters, where similar considerations would apply. The important message is that universal $K_{\Gamma_l}(\mathbf{Q})$ functions, or, more frequently, just the powder-averaged $\bar{K}_{\Gamma_l}(Q)$ functions for the symmetrical systems may describe certain transitions also in systems with lower SPS symmetry.

Truncated tetrahedron. Different types of spin clusters taking the shape of a truncated tetrahedron were synthesized [75,76] but not magnetically characterized in much detail. Classical and quantum-spin models for the antifer-

TABLE XIV. Coefficients $\bar{c}_i^{\Gamma_l}$ defining $\bar{K}_{\Gamma_l}(Q)$ functions for the isotropic cuboctahedron. Site numbers are defined in Fig. 11. For more explanations, see footnote to Table II.

	E_g	T_{2g}	T_{1u}	T_{2u}	$n(t)$
(1, 1)	1	1	1	1	12
(1, 2)	-2	0	2	-2	48
(1, 3)	2	-2	0	0	24
(1, 4)	-2	0	-2	2	48
(1, 5)	1	1	-1	-1	12

romagnetic Heisenberg model were investigated in Refs. [77,78].

We here encounter the case that $\Gamma^{(12)} = A_1 \oplus E \oplus T_1 \oplus 2T_2$ (Table VI) contains T_2 more than once. Therefore no universal function $K_{T_2}(\mathbf{Q})$ exists which would describe transitions $A_1 \rightarrow T_2$ or $A_2 \rightarrow T_1$, cf. Table XI. However, as the number of ferromagnetic molecules studied by INS increases [56,57,79], we chose to still report two different $K_{T_2}(\mathbf{Q})$ for transitions from the “ferromagnetic” A_1 multiplet with $S = S_{\max}$ to the two different T_2 multiplets with $S = S_{\max} - 1$ (unpolarized FCSWT transitions, see Theory section). The $K_{T_2}(\mathbf{Q})$ are still calculated according to Eq. (14) using orthogonal eigenvectors of T_2 states, obtained from diagonalization of the Hamiltonian matrix (effectively the adjacency matrix \mathbf{J} , with nonzero entries of 1 between all interacting sites) in the respective 2×2 subspace. The entries for $T_2(\text{I})$ and $T_2(\text{II})$ in Table XII are identified by the respective eigenvalues J of the adjacency matrix \mathbf{J} (a constant energy shift and multiplication by a constant relates these eigenvalues to energies [63]).

We only plot functions $K_E(\mathbf{Q})$ and $K_{T_1}(\mathbf{Q})$ in Fig. 10. However, apart from a trivial scaling in \mathbf{Q} space required when choosing a different uniform edge length (Fig. 10 refers to $R = 3 \text{ \AA}$), these plots are not universally valid, because there are two topologically inequivalent edges in the

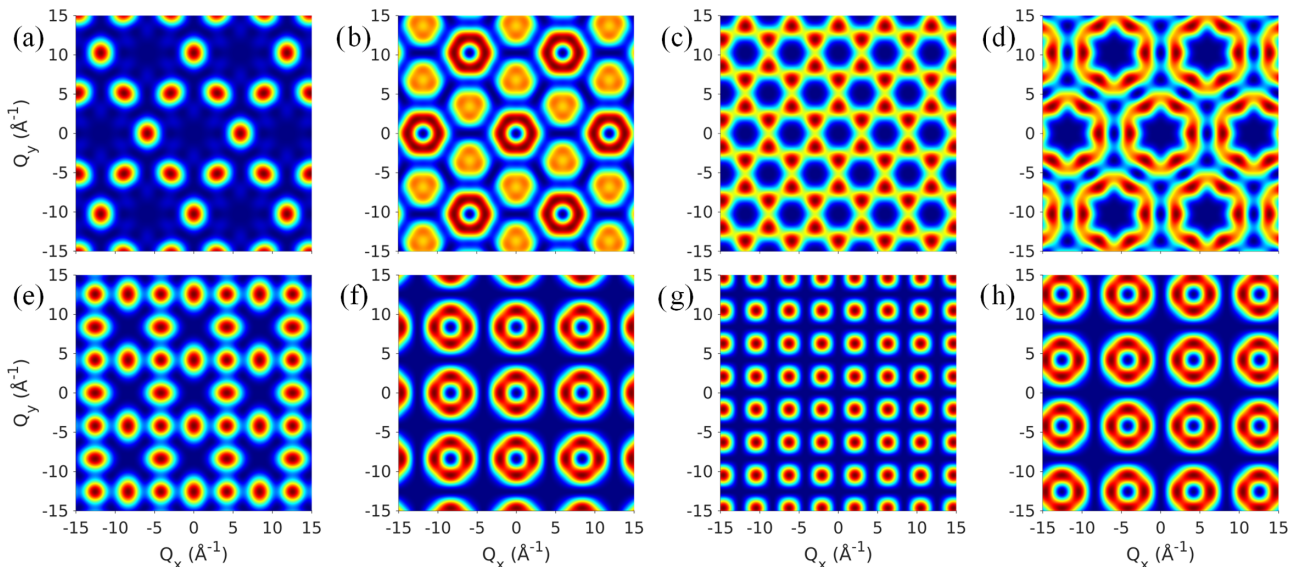


FIG. 12. $K_{\Gamma_l}(\mathbf{Q})$ functions for the cuboctahedron. First row [(a)–(d)]: C_3 axis oriented along z . Second row [(e)–(h)]: C_4 axis oriented along z . In all cases, yz is a mirror plane of the cuboctahedron. The Γ_l label is E_g [(a), (e)], T_{1u} [(b), (f)], T_{2g} [(c), (g)], or T_{2u} [(d), (h)].

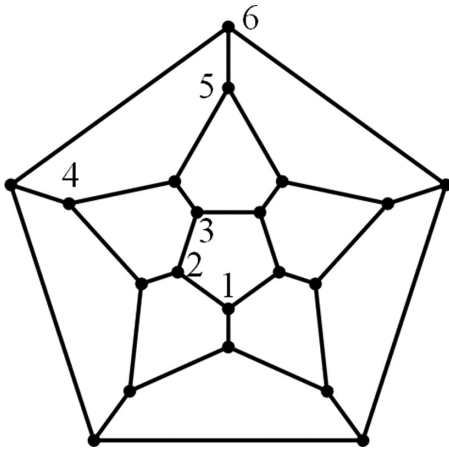


FIG. 13. Schlegel diagram for the dodecahedron. Only sites forming inequivalent pairs with site 1 are numbered.

truncated tetrahedron (the same applies for the truncated icosahedron, Fig. 18). No INS selection rules are expected in the anisotropic truncated tetrahedron, because $\Gamma^{(36)}$ contains all representations at least once (cf. Table VI).

Cuboctahedron. Cuboctahedral molecules comprising 12 Cu^{2+} ions ($s = \frac{1}{2}$) were synthesized [80,81], but no INS experiments were performed yet. Theoretical studies [40,82,83] of the antiferromagnetic Heisenberg model have offered some qualitative insights into aspects pertaining to the kagomé spin lattice. The information on \mathbf{Q} dependencies is contained in Table XIII, Table XIV, Fig. 11, and Fig. 12. The absence of A_{1g} from $\Gamma^{(36)}$ (cf. Table VI) implies that there are a few INS selection rules in an anisotropic cuboctahedron (these are straightforwardly determined and not detailed here).

Dodecahedron. The Heisenberg model on the dodecahedron was discussed in the context of fullerenes [27,61]. A 3D spin configuration corresponding to the classical solution of the Heisenberg model is recovered in *ab initio* generalized Hartree-Fock (GHF) calculations for the smallest fullerene, the C_{20} cage molecule [84]. Full exact diagonal-

TABLE XV. I_h symmetry labels Γ_l specifying $K_{\Gamma_l}(\mathbf{Q})$ functions for unpolarized INS transitions $\Gamma_n \rightarrow \Gamma_m$ in the isotropic spin dodecahedron. For further explanations, see the footnote to Table I.

	A_g	T_{1g}	T_{2g}	F_g	H_g	A_u	T_{1u}	T_{2u}	F_u	H_u
A_g	0	0	0	F_g	H_g	0	T_{1u}	T_{2u}	F_u	0
T_{1g}	0	H_g	N/A	N/A	N/A	T_{1u}	T_{1u}	F_u	N/A	N/A
T_{2g}	0	N/A	H_g	N/A	N/A	T_{2u}	F_u	T_{2u}	N/A	N/A
F_g	F_g	N/A	N/A	N/A	N/A	F_u	N/A	N/A	N/A	N/A
H_g	H_g	N/A	N/A	N/A	N/A	0	N/A	N/A	N/A	N/A
A_u	0	T_{1u}	T_{2u}	F_u	0	0	0	0	F_g	H_g
T_{1u}	T_{1u}	T_{1u}	F_u	N/A	N/A	0	H_g	N/A	N/A	N/A
T_{2u}	T_{2u}	F_u	T_{2u}	N/A	N/A	0	N/A	H_g	N/A	N/A
F_u	F_u	F_u	N/A	N/A	N/A	F_g	N/A	N/A	N/A	N/A
H_u	0	N/A	N/A	N/A	N/A	H_g	N/A	N/A	N/A	N/A

ization for the antiferromagnetic $s = \frac{1}{2}$ dodecahedron and Lanczos exact diagonalization for $s = 1$ revealed some typical features of spin-frustrated systems [35]. A Gd_{20} molecule resembling a dodecahedron and a Gd_{50} Keplerate species where a Gd_{20} dodecahedron encloses a Gd_{30} icosidodecahedron (with approximate I_h symmetry; a similar molecule with a Ni_{30} icosidodecahedron encapsulating a La_{20} dodecahedron has basically ideal I_h symmetry [85,86]) were synthesized recently; their magnetic properties were rationalized based on the classical Heisenberg model [87]. We are not aware of any INS studies for spin dodecahedra. Our results for $K_{\Gamma_l}(\mathbf{Q})$ are summarized in Table XV, Table XVI, Fig. 13, and Fig. 14.

Icosidodecahedron. Antiferromagnetic spin clusters which possess the structure of an icosidodecahedron were realized in terms of the so-called Keplerate molecules $\{\text{Mo}_{72}\text{V}_{30}\}$ [88,89], $\{\text{W}_{72}\text{V}_{30}\}$ [90], $\{\text{Mo}_{72}\text{Cr}_{30}\}$ [91], and $\{\text{Mo}_{72}\text{Fe}_{30}\}$ [92,93], with magnetic ions V^{3+} ($s = \frac{1}{2}$), Cr^{3+} ($s = \frac{3}{2}$), and Fe^{3+} ($s = \frac{5}{2}$), respectively. The rather broad features of powder INS spectra [59] for $\{\text{Mo}_{72}\text{Fe}_{30}\}$ could be partially explained by theoretical analyses [40,59,94]. Our present general results cannot be used to draw additional information from the existing INS data for $\{\text{Mo}_{72}\text{Fe}_{30}\}$ but are expected to

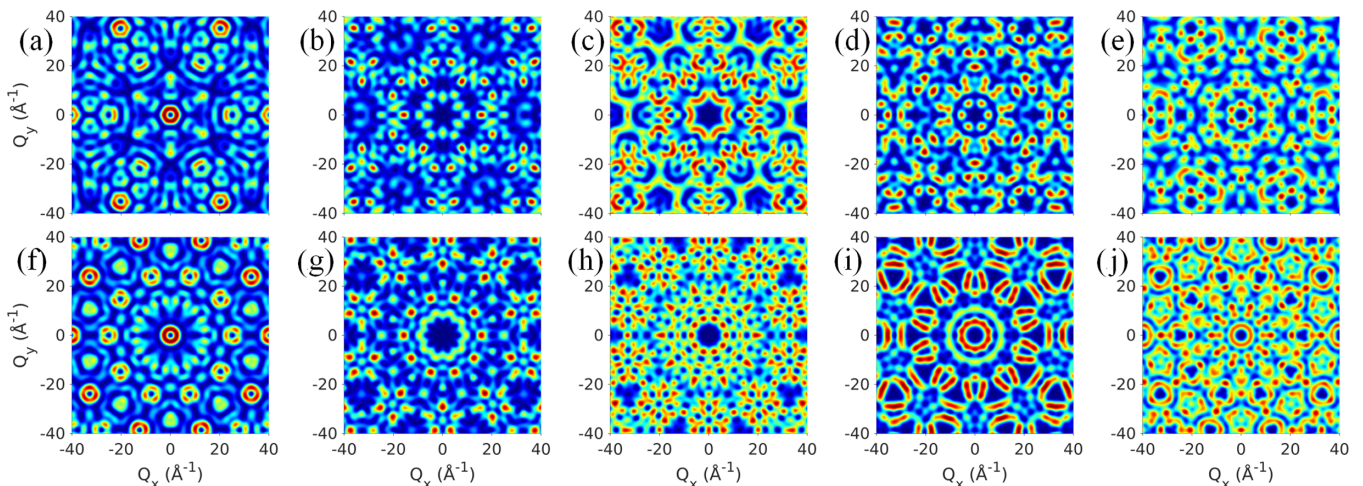


FIG. 14. $K_{\Gamma_l}(\mathbf{Q})$ functions for the dodecahedron. First row [(a)–(e)]: C_3 axis oriented along z . Second row [(f)–(j)]: C_5 axis along z . In all cases, yz is a mirror plane of the dodecahedron. The Γ_l label is T_{1u} [(a), (f)], T_{2u} [(b), (g)], F_g [(c), (h)], F_u [(d), (i)], or H_g [(e), (j)].

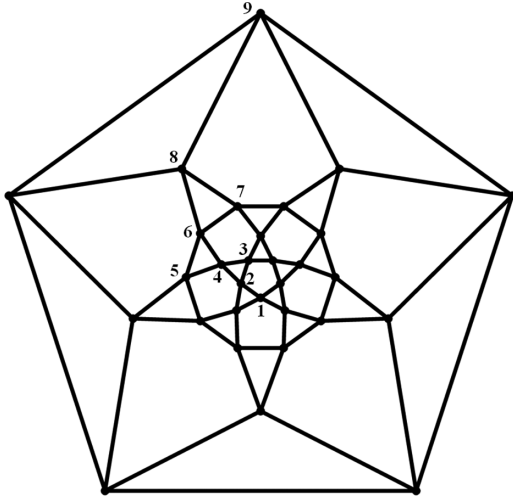


FIG. 15. Schlegel diagram for the icosidodecahedron. Only sites forming inequivalent pairs with site 1 are numbered. The Cartesian distance from site 1 increases with site number.

become useful if higher-resolved spectra of similar molecules are recorded in the future.

In Table XVII we show only those transitions which involve at least one one-dimensional representation of I_h , because none of the transitions between multidimensional representations has a defined universal $K_{\Gamma_l}(\mathbf{Q})$. An $|A_g, S=0\rangle$ or $|A_u, S=0\rangle$ ground state is expected in the antiferromagnetically coupled system [40], and therefore most zero-temperature excitations have a defined $K_{\Gamma_l}(\mathbf{Q})$. The $K_{\Gamma_l}(\mathbf{Q})$ functions are listed in Table XVIII, referring to the pair numbering in Fig. 15. The universal $K_{\Gamma_l}(\mathbf{Q})$ functions are plotted in Fig. 16. It is worth noting that the density matrix renormalization group (DMRG) method reaches its current limits for $s = \frac{5}{2}$ [95]; see also Ref. [96] for a different variational method. Analytical information on \mathbf{Q} dependencies appears valuable, particularly for systems with large s , because exact or approximate eigenvectors are not needed. We finally mention that INS intensities can be estimated by the rather demanding dynamical DMRG technique [97].

Truncated icosahedron. The Heisenberg model on the truncated icosahedron was first discussed in the context of the C_{60} fullerene molecule [70]. As for the dodecahedral C_{20} , the classical 3D spin configuration is recovered in *ab initio* GHF calculations on C_{60} [84]. For antiferromagnetic

TABLE XVI. Coefficients $\bar{c}_l^{\Gamma_l}$ defining $\bar{K}_{\Gamma_l}(Q)$ functions for the isotropic dodecahedron. Site numbers are defined in Fig. 13. For more explanations, see the footnote to Table II.

	T_{1u}	T_{2u}	F_g	F_u	H_g	$n(t)$
(1, 1)	1	1	1	1	1	20
(1, 2)	$\sqrt{5}$	$-\sqrt{5}$	-2	0	1	60
(1, 3)	2	2	1	-3	-2	120
(1, 4)	-2	-2	1	3	-2	120
(1, 5)	$-\sqrt{5}$	$\sqrt{5}$	-2	0	1	60
(1, 6)	-1	-1	1	-1	1	20

TABLE XVII. I_h symmetry labels Γ_l specifying $K_{\Gamma_l}(\mathbf{Q})$ functions for unpolarized INS transitions $\Gamma_n \rightarrow \Gamma_m$ in the isotropic icosidodecahedron. For further explanations, see the footnote to Table I. Only transitions involving at least one one-dimensional representation are given, because all the other transitions would have the entry N/A.

	A_g	T_{1g}	T_{2g}	F_g	H_g	A_u	T_{1u}	T_{2u}	F_u	H_u
A_g	0	0	0	F_g	N/A	0	T_{1u}	T_{2u}	F_u	H_u
A_u	0	T_{1u}	T_{2u}	F_u	H_u	0	0	0	F_g	N/A

TABLE XVIII. Coefficients $\bar{c}_l^{\Gamma_l}$ defining $\bar{K}_{\Gamma_l}(Q)$ functions for the isotropic icosidodecahedron.^a Site numbers are defined in Fig. 15. For more explanations, see footnote to Table II.

	T_{1u}	T_{2u}	F_g	F_u	H_u	$H_g(I)$	$H_g(II)$	$n(t)$
(1, 1)	1	1	1	1	1	1	1	30
(1, 2)	$1 + \sqrt{5}$	$1 - \sqrt{5}$	-1	1	-2	-2	2	120
(1, 3)	2	2	-1	-3	0	1	-1	120
(1, 4)	$-1 + \sqrt{5}$	$-1 - \sqrt{5}$	-1	-1	2	1	-1	120
(1, 5)	0	0	4	0	0	-2	-2	120
(1, 6)	$1 - \sqrt{5}$	$1 + \sqrt{5}$	-1	1	-2	1	-1	120
(1, 7)	-2	-2	-1	3	0	1	-1	120
(1, 8)	$-1 - \sqrt{5}$	$-1 + \sqrt{5}$	-1	-1	2	-2	2	120
(1, 9)	-1	-1	1	-1	-1	1	1	30

^aThe entries for $H_g(I)$ and $H_g(II)$ refer to FC-SWT transitions, with adjacency-matrix eigenvalues of $J[H_g(I)] = -2$ and $J[H_g(II)] = 2$, respectively.

TABLE XIX. I_h symmetry labels Γ_l specifying $K_{\Gamma_l}(\mathbf{Q})$ functions for unpolarized INS transitions $\Gamma_n \rightarrow \Gamma_m$ in the isotropic truncated icosahedron. For further explanations, see the footnote to Table I. Only transitions involving at least one one-dimensional representation are given, because all the other transitions would have the entry N/A.

	A_g	T_{1g}	T_{2g}	F_g	H_g	A_u	T_{1u}	T_{2u}	F_u	H_u
A_g	0	T_{1g}	T_{2g}	N/A	N/A	0	N/A	N/A	N/A	N/A
A_u	0	N/A	N/A	N/A	N/A	0	T_{1g}	T_{2g}	N/A	N/A

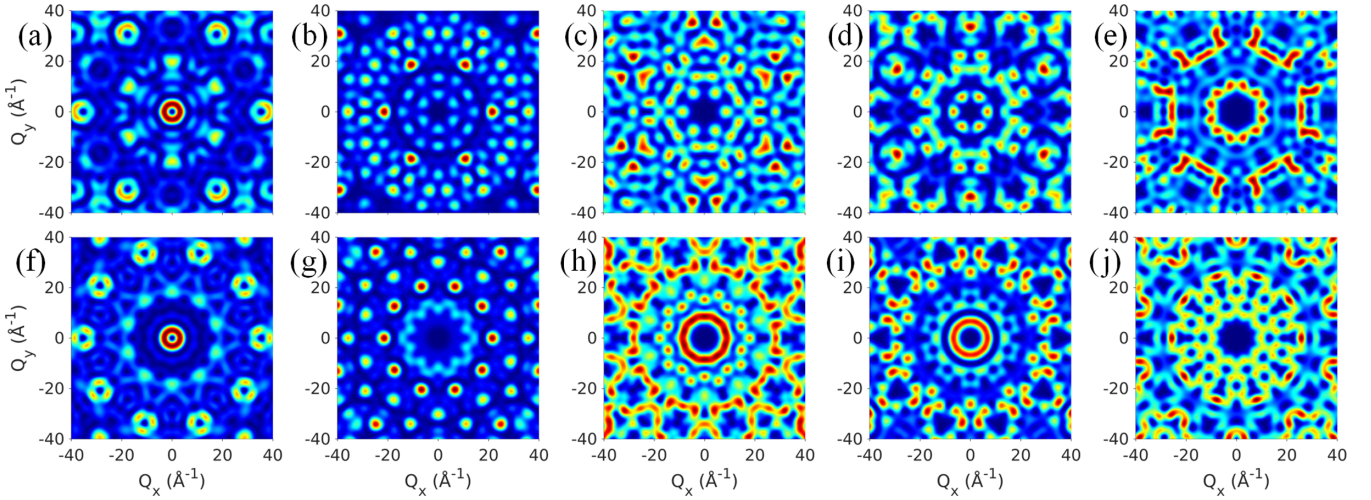


FIG. 16. $K_{\Gamma_l}(\mathbf{Q})$ functions for the icosidodecahedron. First row [(a)–(e)]: C_5 axis oriented along z . Second row [(f)–(j)]: C_3 axis along z . In all cases, yz a mirror plane of the icosidodecahedron. The Γ_l labels are T_{1u} [(a), (f)], T_{2u} [(b), (g)], F_g [(c), (h)], F_u [(d), (i)], or H_u [(e), (j)].

couplings, even the $s = \frac{1}{2}$ system is too large for Lanczos exact diagonalization, and different methods were applied to estimate the ground-state energy variationally [98–100] (most recently by DMRG [101]), or by perturbation theory [70]. As of yet, there apparently exist no spin clusters of this type.

TABLE XX. Coefficients $\bar{c}_i^{\Gamma_l}$ defining $\bar{K}_{\Gamma_l}(Q)$ functions for the isotropic truncated icosahedron. Site numbers are defined in Fig. 17. For more explanations, see footnote to Table II.^a

	$\left\{ \begin{matrix} T_{1g} \\ T_{2g} \end{matrix} \right\}$	$F_g(\text{I})$	$F_g(\text{II})$	$H_g(\text{I})$	$\left\{ \begin{matrix} H_g(\text{II}) \\ H_g(\text{III}) \end{matrix} \right\}$	$n(t)$
J	$\frac{1}{2}(-3 \pm \sqrt{5})$	-2	1	1	$\frac{1}{2}(1 \mp \sqrt{13})$	
(1, 1)	2	3	3	3	78	1
(1, 2)	-2	-2	2	1	$26 \mp 8\sqrt{13}$	1
(1, 3)	$-1 \pm \sqrt{5}$	-4	1	2	$13 \mp 31\sqrt{13}$	2
(1, 4)	$-1 \mp \sqrt{5}$	1	-4	-2	$65 \mp 5\sqrt{13}$	4
(1, 5)	$2 \mp 2\sqrt{5}$	2	-2	-4	$-26 \mp 34\sqrt{13}$	4
(1, 6)	$-1 \pm \sqrt{5}$	1	-4	-2	$65 \pm 13\sqrt{13}$	4
(1, 7)	$2 \pm 2\sqrt{5}$	2	-2	-4	$-26 \pm 2\sqrt{13}$	8
(1, 8)	-2	1	2	-2	$26 \pm 16\sqrt{13}$	4
(1, 9)	4	-8	-4	4	$-52 \pm 16\sqrt{13}$	8
(1, 10)	0	2	10	-4	$-104 \pm 8\sqrt{13}$	8
(1, 11)	$-1 \mp \sqrt{5}$	-4	1	2	$13 \pm 23\sqrt{13}$	8
(1, 12)	-2	6	-3	6	-78	8

^aThe $\bar{K}_{\Gamma_l}(Q)$ functions have universal character for $\Gamma_l = T_{1g}$ and $\Gamma_l = T_{2g}$ only; the other $\bar{K}_{\Gamma_l}(Q)$ refer to FCSWT excitations in a Heisenberg model with a uniform coupling constant between all neighboring sites [cf. Fig. 4(g)]. There is a symmetry about pairs (1,12)–(1,13), $\bar{c}_{1,13} = \bar{c}_{1,12}$, $\bar{c}_{1,14} = \bar{c}_{1,11}$, ..., $\bar{c}_{1,24} = \bar{c}_{1,1}$. This symmetry also holds for the $n(t)$, where we eliminate a common factor of 60 from the $n(t)$ reported in the last column. The J values in the second row are eigenvalues of the adjacency matrix, which are essentially the energies of FCSWT states (in the context of the Hückel model, analytical energy expressions were already reported in Ref. [64]).

There are only two universally valid functions, $K_{T_{1g}}(\mathbf{Q})$ and $K_{T_{2u}}(\mathbf{Q})$, see Table XIX, but we report also $K_{\Gamma_l}(\mathbf{Q})$ functions for all FCSWT transitions in Table XX, Table XXI, and Table XXII. This requires the equivalent of solving the Hückel model on C_{60} in analytical form; analytical expressions for the Hückel eigenvalues are reported in Ref. [64]. Following the numbering of Fig. 17, there is a symmetry in the \bar{c} contributions to $K_{\Gamma_l}(\mathbf{Q})$ about the pairs (1,12)–(1,13), that is, either $\bar{c}_{1,13} = \bar{c}_{1,12}$, $\bar{c}_{1,14} = \bar{c}_{1,11}$, ..., $\bar{c}_{1,24} = \bar{c}_{1,1}$ (symmetric), or $\bar{c}_{1,13} = -\bar{c}_{1,12}$, $\bar{c}_{1,14} = -\bar{c}_{1,11}$, ..., $\bar{c}_{1,24} = -\bar{c}_{1,1}$ (antisymmetric).

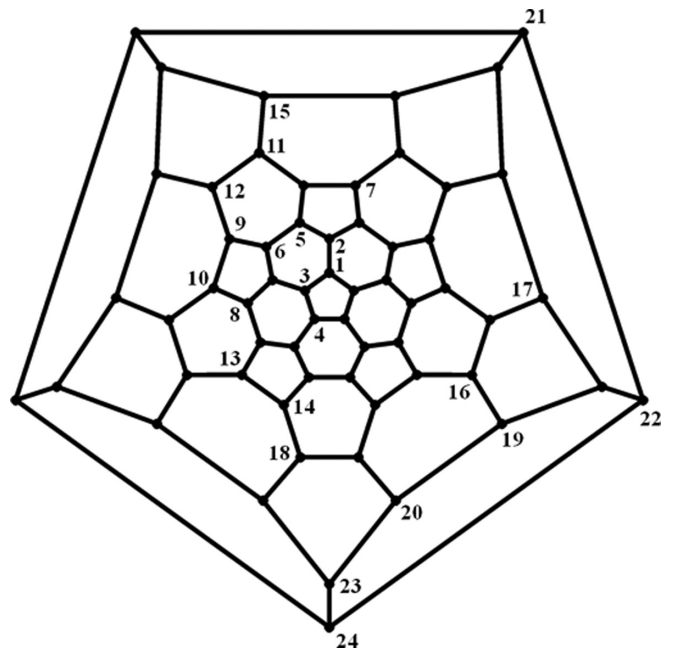


FIG. 17. Schlegel diagram for the truncated icosahedron. Only sites forming inequivalent pairs with site 1 are numbered. The numbering follows Krivnov *et al.* (cf. Fig. 3 in Ref. [99]).

TABLE XXII. Continuation of Table XX. Coefficients are antisymmetric about the pairs (1,12)–(1,13), $\bar{c}_{1,13} = -\bar{c}_{1,12}$, $\bar{c}_{1,14} = -\bar{c}_{1,11}$, ..., $\bar{c}_{1,24} = -\bar{c}_{1,1}$.

J	$\begin{Bmatrix} F_u(\text{I}) \\ F_u(\text{II}) \end{Bmatrix}$	$\begin{Bmatrix} H_u(\text{I}) \\ H_u(\text{II}) \end{Bmatrix}$
J	$-\frac{1}{2}(1 \pm \sqrt{17})$	$-\frac{1}{2}(1 \pm \sqrt{5})$
(1, 1)	34	10
(1, 2)	$\mp 8\sqrt{17}$	$\mp 2\sqrt{5}$
(1, 3)	$-17 \mp 9\sqrt{17}$	$-5 \mp 3\sqrt{5}$
(1, 4)	$-17 \mp 9\sqrt{17}$	$-5 \pm 3\sqrt{5}$
(1, 5)	$68 \pm 8\sqrt{17}$	$-10 \pm 2\sqrt{5}$
(1, 6)	$-17 \mp 7\sqrt{17}$	$-5 \pm 5\sqrt{5}$
(1, 7)	$-68 \pm 8\sqrt{17}$	$10 \pm 2\sqrt{5}$
(1, 8)	$-17 \mp 3\sqrt{17}$	10
(1, 9)	$\pm 8\sqrt{17}$	$\mp 4\sqrt{5}$
(1, 10)	$\pm 4\sqrt{17}$	$\mp 8\sqrt{5}$
(1, 11)	$-17 \mp 7\sqrt{17}$	$-5 \mp 5\sqrt{5}$
(1, 12)	$-17 \pm 3\sqrt{17}$	10

In Fig. 18 the universally valid functions $K_{\Gamma_l}(\mathbf{Q})$ with $\Gamma_l = T_{1g}$ and $\Gamma_l = T_{2g}$ are plotted. All irreducible representations occur at least once in $\Gamma^{(180)}$ (Table VI). Therefore anisotropic interactions are expected to lift all INS selection rules in the truncated icosahedron.

IV. CONCLUSIONS

We have shown how the point-group symmetry of molecular spin clusters can impose selection rules on inelastic neutron scattering (INS) transitions. Selection rules are obtained based on a decomposition of the set of local spin operators in terms of irreducible representations of the point

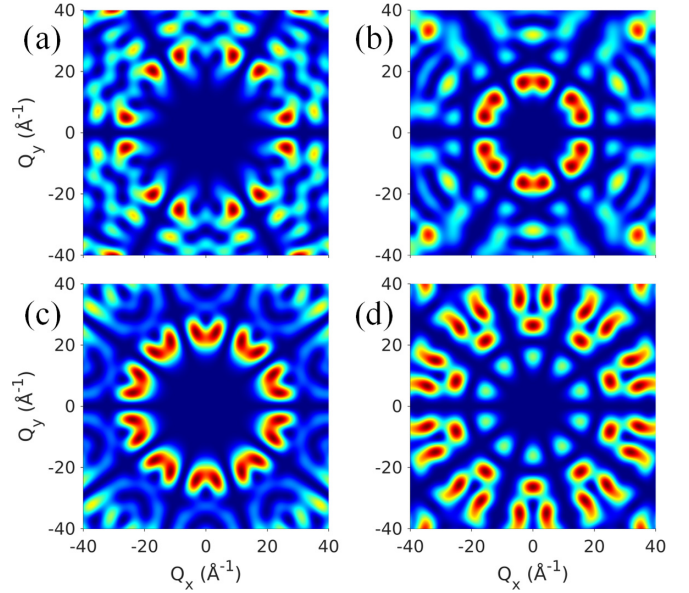


FIG. 18. $K_{\Gamma_l}(\mathbf{Q})$ functions for the truncated icosahedron. First row [(a), (b)]: C_3 axis oriented along z . Second row [(c), (d)]: C_5 axis along z . In all cases, yz is a mirror plane of the truncated icosahedron. The Γ_l label is T_{1g} [(a), (b)] or T_{2g} [(c), (d)].

group. Spin-permutational symmetry must be considered for isotropic systems, while for anisotropic systems the combination of permutation and rotation operations requires one to take into account the vector character of spin operators.

The huge potential of 4D-INS spectroscopy makes it highly likely that additional spin clusters will be characterized by this technique in the future. An efficient accumulation and simulation of data should profit from clearly separating those features that are determined by symmetry from those that

TABLE XXI. Continuation of Table XX. Coefficients are antisymmetric about the pairs (1,12)–(1,13), $\bar{c}_{1,13} = -\bar{c}_{1,12}$, $\bar{c}_{1,14} = -\bar{c}_{1,11}$, ..., $\bar{c}_{1,24} = -\bar{c}_{1,1}$.

J	$\begin{Bmatrix} T_{1u}(\text{I}) \\ T_{1u}(\text{II}) \end{Bmatrix}$	$\begin{Bmatrix} T_{2u}(\text{I}) \\ T_{2u}(\text{II}) \end{Bmatrix}$
J	$\frac{1}{4}[3 + \sqrt{5} \mp \sqrt{38-2\sqrt{5}}]$	$\frac{1}{4}[3 - \sqrt{5} \mp \sqrt{38 + 2\sqrt{5}}]$
(1, 1)	356	356
(1, 2)	$\mp 4\sqrt{89(37 + 16\sqrt{5})}$	$\mp 4\sqrt{89(37 - 16\sqrt{5})}$
(1, 3)	$89(3 + \sqrt{5}) \mp \sqrt{178(919 - 317\sqrt{5})}$	$89(3 - \sqrt{5}) \mp \sqrt{178(919 + 317\sqrt{5})}$
(1, 4)	$89(3 - \sqrt{5}) \mp \sqrt{178(839 + 269\sqrt{5})}$	$89(3 + \sqrt{5}) \mp \sqrt{178(839 - 269\sqrt{5})}$
(1, 5)	$178(-1 + \sqrt{5}) \mp 2\sqrt{178(499 + 233\sqrt{5})}$	$178(-1 - \sqrt{5}) \mp 2\sqrt{178(499 - 233\sqrt{5})}$
(1, 6)	$89(3 + \sqrt{5}) \mp \sqrt{178(1031 - 461\sqrt{5})}$	$89(3 - \sqrt{5}) \pm \sqrt{178(1031 + 461\sqrt{5})}$
(1, 7)	$178(1 + \sqrt{5}) \mp 2\sqrt{178(19 + \sqrt{5})}$	$178(1 - \sqrt{5}) \mp 2\sqrt{178(19 - \sqrt{5})}$
(1, 8)	$-2(89 \pm \sqrt{89(593 + 64\sqrt{5})})$	$-2(89 \mp \sqrt{89(593 - 64\sqrt{5})})$
(1, 9)	$4(89\sqrt{5} \pm \sqrt{89(37 + 16\sqrt{5})})$	$4(-89\sqrt{5} \pm \sqrt{89(37 - 16\sqrt{5})})$
(1, 10)	$\mp 16\sqrt{89(13 - 4\sqrt{5})}$	$\pm 16\sqrt{89(13 + 4\sqrt{5})}$
(1, 11)	$89(3 - \sqrt{5}) \mp \sqrt{178(151 - 67\sqrt{5})}$	$89(3 + \sqrt{5}) \pm \sqrt{178(151 + 67\sqrt{5})}$
(1, 12)	$-2(89 \pm \sqrt{89(193 - 32\sqrt{5})})$	$-2(89 \mp \sqrt{89(193 + 32\sqrt{5})})$

contain nonredundant dynamical information. We have here provided a generalized discussion of how the dependence of the INS cross section on the momentum-transfer vector \mathbf{Q} is under certain conditions completely determined by the symmetry species of the states involved in a transition, an issue that had so far been detailed only for cyclic spin systems. In the present work, INS selection rules and \mathbf{Q} dependencies were discussed for spin rings and a number of cubic and icosahedral spin polyhedra. Analytical expressions for universal \mathbf{Q} -dependent intensity functions were tabulated. For small isotropic polyhedra (e.g., cuboctahedron, icosahedron, etc.), many types of transitions have symmetry-determined \mathbf{Q}

dependencies; there still exist a few transitions with universal \mathbf{Q} dependencies in the truncated icosahedron. In such cases, only the absolute INS intensity contains information on the spin dynamics, thereby affording a clear separation of geometrical and dynamical effects. Overall, we hope this work will provide additional motivation to further pursue the synthesis and subsequent INS characterization of spin clusters of high molecular symmetry.

ACKNOWLEDGMENT

The author thanks Martin Kaupp for generous support.

- [1] A. Bencini and D. Gatteschi, *Electron Paramagnetic Resonance of Exchange Coupled Systems* (Springer-Verlag, Berlin, 1990).
- [2] D. Gatteschi and R. Sessoli, *Angew. Chemie Int. Ed.* **42**, 268 (2003).
- [3] J. Schnack, *Contemp. Phys.* **60**, 127 (2019).
- [4] M. N. Leuenberger and D. Loss, *Nature (London)* **410**, 789 (2001).
- [5] J. Ferrando-Soria, E. M. Pineda, A. Chiesa, A. Fernandez, S. A. Magee, S. Carretta, P. Santini, I. J. Vitorica-Yrezabal, F. Tuna, G. A. Timco *et al.*, *Nat. Commun.* **7**, 11377 (2016).
- [6] C. Godfrin, A. Ferhat, R. Ballou, S. Klyatskaya, M. Ruben, W. Wernsdorfer, and F. Balestro, *Phys. Rev. Lett.* **119**, 187702 (2017).
- [7] A. Gaita-Ariño, F. Luis, S. Hill, and E. Coronado, *Nat. Chem.* **11**, 301 (2019).
- [8] M. Atzori and R. Sessoli, *J. Am. Chem. Soc.* **141**, 11339 (2019).
- [9] A. Chiesa, E. Macaluso, F. Petiziol, S. Wimberger, P. Santini, and S. Carretta, *J. Phys. Chem. Lett.* **11**, 8610 (2020).
- [10] G. Christou, D. Gatteschi, D. N. Hendrickson, and R. Sessoli, *MRS Bull.* **25**, 66 (2000).
- [11] C. A. P. Goodwin, F. Ortu, D. Reta, N. F. Chilton, and D. P. Mills, *Nature (London)* **548**, 439 (2017).
- [12] F.-S. Guo, B. M. Day, Y.-C. Chen, and M.-L. Tong, *Science* **362**, 1400 (2018).
- [13] M. Evangelisti and E. K. Brechin, *J. Chem. Soc., Dalton Trans.* **39**, 4672 (2010).
- [14] L. Bogani and W. Wernsdorfer, *Nat. Mater.* **7**, 179 (2008).
- [15] H. U. Güdel and A. Furrer, *Mol. Phys.* **33**, 1335 (1977).
- [16] A. Furrer and H. U. Güdel, *Phys. Rev. Lett.* **39**, 657 (1977).
- [17] A. Furrer and H. U. Güdel, *J. Magn. Magn. Mater.* **14**, 256 (1979).
- [18] R. Basler, C. Boskovic, G. Chaboussant, H. U. Güdel, M. Murre, S. T. Ochsenein, and A. Sieber, *ChemPhysChem* **4**, 910 (2003).
- [19] G. Amoretti, R. Caciuffo, S. Carretta, T. Guidi, N. Magnani, and P. Santini, *Inorg. Chim. Acta* **361**, 3771 (2008).
- [20] A. Furrer and O. Waldmann, *Rev. Mod. Phys.* **85**, 367 (2013).
- [21] M. L. Baker, S. J. Blundell, N. Domingo, and S. Hill, Spectroscopy methods for molecular nanomagnets, in *Molecular Nanomagnets and Related Phenomena*, edited by S. Gao (Springer, Berlin, Heidelberg, 2015), pp. 231–291.
- [22] E. Garlatti, A. Chiesa, T. Guidi, G. Amoretti, P. Santini, and S. Carretta, *Eur. J. Inorg. Chem.* **2019**, 1106 (2019).
- [23] O. Waldmann, R. Bircher, G. Carver, A. Sieber, H. U. Güdel, and H. Mutka, *Phys. Rev. B* **75**, 174438 (2007).
- [24] M. L. Baker, T. Guidi, S. Carretta, J. Ollivier, H. Mutka, H. U. Güdel, G. A. Timco, E. J. L. McInnes, G. Amoretti, R. E. P. Winpenny *et al.*, *Nat. Phys.* **8**, 906 (2012).
- [25] E. Garlatti, T. Guidi, S. Ansbro, P. Santini, G. Amoretti, J. Ollivier, H. Mutka, G. Timco, I. J. Vitorica-Yrezabal, G. F. S. Whitehead *et al.*, *Nat. Commun.* **8**, 14543 (2017).
- [26] A. Chiesa, T. Guidi, S. Carretta, S. Ansbro, G. A. Timco, I. Vitorica-Yrezabal, E. Garlatti, G. Amoretti, R. E. P. Winpenny, and P. Santini, *Phys. Rev. Lett.* **119**, 217202 (2017).
- [27] E. Garlatti, T. Guidi, A. Chiesa, S. Ansbro, M. L. Baker, J. Ollivier, H. Mutka, G. A. Timco, I. Vitorica-Yrezabal, E. Pavarini *et al.*, *Chem. Sci.* **9**, 3555 (2018).
- [28] E. Garlatti, L. Tesi, A. Lunghi, M. Atzori, D. J. Voneshen, P. Santini, S. Sanvito, T. Guidi, R. Sessoli, and S. Carretta, *Nat. Commun.* **11**, 1751 (2020).
- [29] A. Chiesa, F. Tacchino, M. Grossi, P. Santini, I. Tavernelli, D. Gerace, and S. Carretta, *Nat. Phys.* **15**, 455 (2019).
- [30] S. Ghassemi Tabrizi, A. V. Arbuznikov, and M. Kaupp, *J. Phys. Chem. A* **120**, 6864 (2016).
- [31] O. Waldmann, *Phys. Rev. B* **61**, 6138 (2000).
- [32] O. Waldmann, *Phys. Rev. B* **68**, 174406 (2003).
- [33] B. S. Tsukerblat, *Group Theory in Chemistry and Spectroscopy*, 2nd ed. (Dover Publications, New York, 2006).
- [34] C. Raghu, I. Rudra, D. Sen, and S. Ramasesha, *Phys. Rev. B* **64**, 064419 (2001).
- [35] N. P. Konstantinidis, *Phys. Rev. B* **72**, 064453 (2005).
- [36] J. J. Borrás-Almenar, J. M. Clemente-Juan, E. Coronado, and B. S. Tsukerblat, *Inorg. Chem.* **38**, 6081 (1999).
- [37] R. Schnalle and J. Schnack, *Int. Rev. Phys. Chem.* **29**, 403 (2010).
- [38] T. Heitmann and J. Schnack, *Phys. Rev. B* **99**, 134405 (2019).
- [39] S. Ghassemi Tabrizi, A. V. Arbuznikov, and M. Kaupp, *Chem. Eur. J.* **24**, 4689 (2018).
- [40] I. Rousochatzakis, A. M. Läuchli, and F. Mila, *Phys. Rev. B* **77**, 094420 (2008).
- [41] N. P. Konstantinidis, *J. Phys.: Condens. Matter* **27**, 76001 (2015).
- [42] T. Moriya, *Phys. Rev.* **120**, 91 (1960).
- [43] R. A. Klemm and D. V. Efremov, *Phys. Rev. B* **77**, 184410 (2008).
- [44] S. Ghassemi Tabrizi, TU Berlin, Ph.D. Dissertation, 2017.
- [45] W. Marshall and S. W. Lovesey, *Theory of Thermal Neutron Scattering* (Clarendon Press, Oxford, 1971).

- [46] K. Riedl, D. Guterding, H. O. Jeschke, M. J. P. Gingras, and R. Valentí, *Phys. Rev. B* **94**, 014410 (2016).
- [47] H. U. Güdel, U. Hauser, and A. Furrer, *Inorg. Chem.* **18**, 2730 (1979).
- [48] J. T. Haraldsen, T. Barnes, and J. L. Musfeldt, *Phys. Rev. B* **71**, 064403 (2005).
- [49] J. T. Haraldsen, *Phys. Rev. Lett.* **107**, 037205 (2011).
- [50] A. Roxburgh and J. T. Haraldsen, *Phys. Rev. B* **98**, 214434 (2018).
- [51] P. W. Atkins and R. S. Friedman, *Molecular Quantum Mechanics* (Oxford University Press, Oxford, 2011).
- [52] J. S. Griffith, *The Irreducible Tensor Method for Molecular Symmetry Groups* (Prentice-Hall, Englewood Cliffs, NJ, 1962).
- [53] S. L. Altmann and P. Herzog, *Point-Group Theory Tables* (Clarendon Press, Oxford, 1994).
- [54] E. U. Condon and H. Odabaşı, *Atomic Structure* (Cambridge University Press, London, 1980).
- [55] K. Prša and O. Waldmann, *Inorganics* **6**, 49 (2018).
- [56] K. Prša and O. Waldmann, *Eur. J. Inorg. Chem.* **2019**, 1128 (2019).
- [57] S. Nekuruh, J. Nehrkor, K. Prša, J. Dreiser, A. M. Ako, C. E. Anson, T. Unruh, A. K. Powell, and O. Waldmann, *Inorg. Chem.* **58**, 11256 (2019).
- [58] J. Schnack, *J. Chem. Soc., Dalton Trans.* **39**, 4677 (2010).
- [59] V. O. Garlea, S. E. Nagler, J. L. Zarestky, C. Stassis, D. Vaknin, P. Kögerler, D. F. McMorro, C. Niedermayer, D. A. Tennant, B. Lake *et al.*, *Phys. Rev. B* **73**, 024414 (2006).
- [60] J. T. Haraldsen, *Phys. Rev. B* **94**, 054436 (2016).
- [61] M. Tinkham, *Group Theory and Quantum Mechanics* (McGraw-Hill, New York, 1964).
- [62] J. J. Sakurai, *Modern Quantum Mechanics*, 2nd ed., edited by San Fu Tuan (Addison Wesley, Reading, MA, 1993).
- [63] H.-J. Schmidt and M. Luban, *J. Phys. A* **36**, 6351 (2003).
- [64] W. B. Brown, *Chem. Phys. Lett.* **136**, 128 (1987).
- [65] R. E. Stanton and M. D. Newton, *J. Phys. Chem.* **92**, 2141 (1988).
- [66] E. J. Schelter, F. Karadas, C. Avendano, A. V. Prosvirin, W. Wernsdorfer, and K. R. Dunbar, *J. Am. Chem. Soc.* **129**, 8139 (2007).
- [67] M. Nihei, M. Ui, N. Hoshino, and H. Oshio, *Inorg. Chem.* **47**, 6106 (2008).
- [68] R. J. Holmberg, M. Kay, I. Korobkov, E. Kadantsev, P. G. Boyd, T. Aharen, S. Desgreniers, T. K. Woo, and M. Murugesu, *Chem. Commun.* **50**, 5333 (2014).
- [69] C. Schröder, H.-J. Schmidt, J. Schnack, and M. Luban, *Phys. Rev. Lett.* **94**, 207203 (2005).
- [70] D. Coffey and S. A. Trugman, *Phys. Rev. Lett.* **69**, 176 (1992).
- [71] N. P. Konstantinidis, *Phys. Rev. B* **76**, 104434 (2007).
- [72] E. I. Tolis, L. P. Engelhardt, P. V. Mason, G. Rajaraman, K. Kindo, M. Luban, A. Matsuo, H. Nojiri, J. Raftery, C. Schröder *et al.*, *Chem. Eur. J.* **12**, 8961 (2006).
- [73] D. Vaknin and F. Demmel, *Phys. Rev. B* **89**, 180411 (2014).
- [74] L. Engelhardt, F. Demmel, M. Luban, G. A. Timco, F. Tuna, and R. E. P. Winpenny, *Phys. Rev. B* **89**, 214415 (2014).
- [75] C. P. Pradeep, D.-L. Long, P. Kögerler, and L. Cronin, *Chem. Commun.* **41**, 4254 (2007).
- [76] Y. Zheng, Q.-C. Zhang, L.-S. Long, R.-B. Huang, A. Müller, J. Schnack, L.-S. Zheng, and Z. Zheng, *Chem. Commun.* **49**, 36 (2013).
- [77] D. Coffey and S. A. Trugman, *Phys. Rev. B* **46**, 12717 (1992).
- [78] R. Schnalle and J. Schnack, *Phys. Rev. B* **79**, 104419 (2009).
- [79] Z. Fu, L. Qin, K. Sun, L. Hao, Y.-Z. Zheng, W. Lohstroh, G. Günther, M. Russina, Y. Liu, Y. Xiao *et al.*, *npj Quantum Mater.* **5**, 32 (2020).
- [80] A. J. Blake, R. O. Gould, C. M. Grant, P. E. Y. Milne, S. Parsons, and R. E. P. Winpenny, *J. Chem. Soc., Dalton Trans.* **4**, 485 (1997).
- [81] M. A. Palacios, E. Moreno Pineda, S. Sanz, R. Inglis, M. B. Pitak, S. J. Coles, M. Evangelisti, H. Nojiri, C. Heesing, E. K. Brechin *et al.*, *ChemPhysChem* **17**, 55 (2016).
- [82] J. Schnack, H.-J. Schmidt, J. Richter, and J. Schulenburg, *Eur. Phys. J. B* **24**, 475 (2001).
- [83] J. Schnack and R. Schnalle, *Polyhedron* **28**, 1620 (2009).
- [84] C. A. Jiménez-Hoyos, R. Rodríguez-Guzmán, and G. E. Scuseria, *J. Phys. Chem. A* **118**, 9925 (2014).
- [85] X.-J. Kong, Y.-P. Ren, L.-S. Long, Z. Zheng, R.-B. Huang, and L.-S. Zheng, *J. Am. Chem. Soc.* **129**, 7016 (2007).
- [86] X.-J. Kong, L.-S. Long, Z. Zheng, R.-B. Huang, and L.-S. Zheng, *Acc. Chem. Res.* **43**, 201 (2010).
- [87] L. Qin, G.-J. Zhou, Y.-Z. Yu, H. Nojiri, C. Schröder, R. E. P. Winpenny, and Y.-Z. Zheng, *J. Am. Chem. Soc.* **139**, 16405 (2017).
- [88] A. Müller, A. M. Todea, J. van Slageren, M. Dressel, H. Bögge, M. Schmidtman, M. Luban, L. Engelhardt, and M. Rusu, *Angew. Chemie* **117**, 3925 (2005).
- [89] B. Botar, P. Kögerler, and C. L. Hill, *Chem. Commun.* 3138 (2005), doi: 10.1039/b504491j.
- [90] A. M. Todea, A. Merca, H. Bögge, T. Glaser, L. Engelhardt, R. Prozorov, M. Luban, and A. Müller, *Chem. Commun.* 3351 (2009), doi: 10.1039/b907188a.
- [91] A. M. Todea, A. Merca, H. Bögge, J. van Slageren, M. Dressel, L. Engelhardt, M. Luban, T. Glaser, M. Henry, and A. Müller, *Angew. Chemie Int. Ed.* **46**, 6106 (2007).
- [92] A. Müller, S. Sarkar, S. Q. N. Shah, H. Bögge, M. Schmidtman, S. Sarkar, P. Kögerler, B. Hauptfleisch, A. X. Trautwein, and V. Schünemann, *Angew. Chem. Int. Ed.* **38**, 3238 (1999).
- [93] A. Müller, M. Luban, C. Schröder, R. Modler, P. Kögerler, M. Axenovich, J. Schnack, P. Canfield, S. Bud'ko, and N. Harrison, *ChemPhysChem* **2**, 517 (2001).
- [94] O. Waldmann, *Phys. Rev. B* **75**, 012415 (2007).
- [95] J. Ummethum, J. Schnack, and A. M. Läuchli, *J. Magn. Magn. Mater.* **327**, 103 (2013).
- [96] E. Neuscamman and G. K.-L. Chan, *Phys. Rev. B* **86**, 064402 (2012).
- [97] J. Ummethum, J. Nehrkor, S. Mukherjee, N. B. Ivanov, S. Stuibler, T. Strässle, P. L. W. Tregenna-Piggott, H. Mutka, G. Christou, O. Waldmann *et al.*, *Phys. Rev. B* **86**, 104403 (2012).
- [98] D. N. Sheng, Z. Y. Weng, C. S. Ting, and J. M. Dong, *Phys. Rev. B* **49**, 4279 (1994).
- [99] V. Y. Krivnov, I. L. Shamovsky, E. E. Tornau, and A. Rosengren, *Phys. Rev. B* **50**, 12144 (1994).
- [100] N. Flocke, T. G. Schmalz, and D. J. Klein, *J. Chem. Phys.* **109**, 873 (1998).
- [101] R. Rausch, C. Plorin, and M. Peschke, arXiv:2011.12083.